ACS MATERIALS Au
AN OPEN ACCESS JOURNAL OF THE AMERICAN CHEMICAL SOCIETY

pubs.acs.org/materialsau Review

Roles of Graphene Oxide in Heterogeneous Photocatalysis

Kang-Qiang Lu,* Yue-Hua Li, Zi-Rong Tang, and Yi-Jun Xu*

Cite This: ACS Mater. Au 2021, 1, 37−54 Read Online

ACCESS | Metrics & More | Article Recommendations

ABSTRACT: Graphene oxide (GO) has been widely utilized as the precursor of graphene (GR) to fabricate GR-based hybrid photocatalysts for solar-to-chemical energy conversion. However, until now, the properties and roles that GO played in heterogeneous photocatalysis have remained relatively elusive. In this Review, we start with a brief discussion of synthesis and structure of GO. Then, the photocatalysis-related properties of GO, including electrical conductivity, surface chemistry, dispersibility, and semiconductor properties, are concisely summarized. In particular, we have highlighted the fundamental multifaceted roles of GO in heterogeneous photocatalysis, which contain the precursor of GR, cross-linked framework for constructing aerogel photocatalyst, macromolecular surfactant, two-dimensional growth template, and photocatalyst by itself. Furthermore, the future prospects and remaining challenges on developing effective GO-derived hybrid photocatalysts are presented, which is expected to inspire further research into this promising research domain.

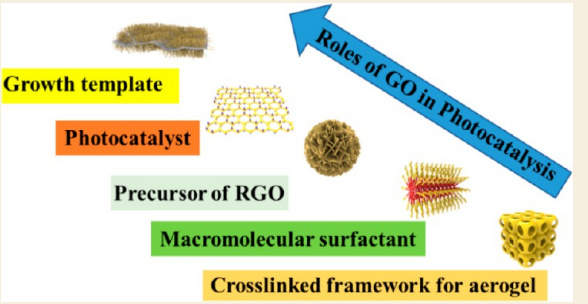

1. INTRODUCTION

Solar-to-chemical energy conversion through photocatalytic technology has attracted wide attention because it offers a promising solution to the energy crisis and environmental pollution issues.[1−6] Up to now, various semiconductor-based photocatalysts have been synthesized and applied for different reactions, including H_2 evolution from water splitting, CO_2 reduction to value-added chemicals, atmospheric ammonia synthesis, pollutant elimination, and organic synthesis.[7−13] Nevertheless, one of the crucial problems limiting the application of semiconductor-based photocatalysts is that photogenerated charge carriers in the excited state are unstable and easily recombined, which leads to a relatively inferior performance of semiconductor photocatalysts.[14−16] Therefore, enhancing the separation and migration of photoinduced electron−hole pairs is a significant and challenging theme to boost the performance of semiconductor-based photocatalysts for target reactions.[17−19]

Compositing semiconductors with graphene (GR) is considered as a viable strategy to boost the performance of semiconductors because the superior conductivity of GR enables it to efficiently accept and conduct photoinduced electrons from semiconductors.[20−23] Therefore, the more effective separation of photogenerated electron−hole pairs is beneficial to improve the photocatalytic activity of semiconductors.[24−26] Regarding the synthesis of GR-based semiconductor hybrid, graphene oxide (GO), on account of its high yield, abundant surface functional groups, and flexible solution processability, has been frequently used as the precursor of GR.[27−29] Because of the unique structure and surface chemistry features, the roles of GO played in heterogeneous photocatalysis are found to be diverse.[11,30] For example, except for the role as precursor to synthesize GR, GO can also act as "macromolecular surfactants" to promote the dispersion of insoluble materials.[31−33] The two-dimensional (2D) structure allows GO to serve as a growth template to induce the synthesis of composite materials with special morphology.[34−36] In addition, GO can also be used as a building block for the preparation of three-dimensional (3D) GR aerogel-supported photocatalysts.[37−39] Furthermore, GO with appropriate degree of oxidation can be directly used as a photocatalyst for various redox reactions.[40,41] There have been some excellent reviews on preparation and applications of GR-based composite photocatalysts.[42−47] However, to the best of our knowledge, an integral overview that focuses on synthesis, properties, and multifarious roles of GO in heterogeneous photocatalysis has been still unavailable. Therefore, it is imperative to compile a general review from the widely dispersed literature to provide useful information and stimulate further development in this significant field.

In this Review, we first briefly reveal the synthesis methods and structural features of GO. Then, photocatalysis-related properties of GO, including electrical conductivity, surface

Received: June 27, 2021
Published: August 9, 2021

chemistry, dispersibility, and semiconductor properties, have been summarized. Next, we put dedicated emphasis on the multifarious roles of GO in heterogeneous photocatalysis, which contain precursor of GR, cross-linked framework for constructing aerogel photocatalyst, macromolecular surfactant, 2D growth template, and photocatalyst (Figure 1). Finally, the

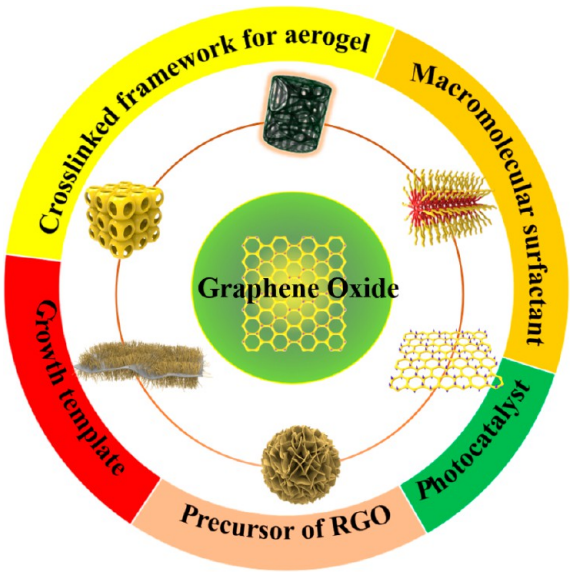

Figure 1. Schematic illustration of multifarious roles of GO in heterogeneous photocatalysis.

prospective research tendencies and challenges of constructing GO-derived photocatalysts for solar energy conversion are presented. This Review is expected to furnish salutary information for in-depth understanding of the diverse roles of GO in photocatalysis, thus promoting ongoing interest in rational utilization of the unique structure and properties of GO to construct high-performance GR-based photocatalysts toward target applications.

2. SYNTHESIS AND STRUCTURE OF GRAPHENE OXIDE

2.1. Synthesis

Similar to GR obtained by stripping graphite, GO can be obtained by stripping graphite oxide.[48−51] Brodie first reported the preparation of graphite oxide from original graphite in 1859.[52] In comparison, the preparations of graphite oxides have only been activated in the past decade, mainly because of the initiative contributions of Ruoff et al.[53−55] As shown in Table 1, some typical methods for GO synthesis are summarized, and their advantages and disadvantages are discussed. Notably, in 1958, Hummers reported the most commonly used method today: graphite by oxidation treating with $KMnO_4$ and $NaNO_3$ in concentrated H_2SO_4.[56,57] It can be found that the Hummers oxidation method is more efficient and safer than Brodie and Staudenmaier methods. Nevertheless, further improvements of the Hummers method are highly required because this method will release toxic gases (NO_2, N_2O_4) during the oxidation process.[58−60] To address this problem, some modified Hummers methods have been proposed.[61] For example, in 2010, Tour reported an improved Hummers method by replacing HNO_3 with the less corrosive H_3PO_4.[56] This modified Hummers method can not only address the problem of toxic gas release but also synthesize GO with higher degree of oxidization and fewer defects in the basal plane, which makes it attractive to efficiently produce high-quality GO. In addition, the Hummers method has another inherent limitation associated with the explosive risk of permanganate oxidants. In recent years, this problem can be partially solved by using relatively mild oxidants, such as K_2FeO_4.[62] As presented in Figure 2, the oxidation treatment of graphite makes graphite sheets contain abundant oxygenated functional groups, which increases the distance and reduces the van der Waals force between graphite layers, thus promoting the exfoliation of graphite oxide.[1,63,64] GO can be finally obtained by mechanical stirring or ultrasonic treatment of graphite oxide in polar organic solvent or water medium.[65−67]

Table 1. Various Synthesis Methods of GO

name	oxidizing agents/steps	advantages	disadvantages	year[ref]
Brodie	$KClO_3$ + HNO_3, 60 °C, 4 days	first synthetic method	request to repeat four oxidation steps	1859[52]
Staudenmaier	$KClO_3$ + HNO_3 + H_2SO_4	simpler and more efficient than Brodie method	production of toxic gases	1898[68]
Hofmann	same as Staudenmaier method, but with HNO_3	avoid the usage of corrosive HNO_3	production of toxic gases (NO_x)	1937[69]
Hummers and Offeman	$NaNO_3$ + $KMnO_4$ + H_2SO_4, 45 °C, 2 h	avoid the usage of corrosive HNO_3	production of toxic gases (NO_x)	1958[57]
Kovtyukhova	(i) H_2SO_4 + $K_2S_2O_8$, P_2O_5, 80 °C, 6 h (ii) H_2SO_4 + $KMnO_4$, 35 °C, 2 h (iii) 30% H_2O_2	high level of oxidation	multiple steps and production of toxic gases (NO_x)	1999[70]
Modified Hummers method by Hirata	(i) H_2SO_4 + $KMnO_4$ + $NaNO_3$, 20 °C, 5 days (ii) 30% H_2O_2	high yield	long oxidation reaction	2004[71]
Ang and Loh	(i) $NaNO_3$ + H_2SO_4 + $KMnO_4$, 90 °C, 0.5 h (ii) redisperse in DMF + tetrabutyl ammonium hydroxide + H_2O, 90 °C, 2 day	high GO content, more than 90% monolayer	long duration, multiple steps	2009[72]
Marcano and Tour	(i) $KMnO_4$ + H_2SO_4 + H_3PO_4, 50 °C, 12 h. (ii) 30% H_2O_2	no poisonous gas production	creating explosive Mn_2O_7 intermediates	2010[56,73]
Eigler	(i) $NaNO_3$ + H_2SO_4 + $KMnO_4$, 30 °C, 21 h (ii) 30% H_2O_2	minimum CO_2 production	generation of poisonous gases (NO_x)	2013[74]
Peng-Gao	K_2FeO_4 + H_2SO_4, room temperature, 1 h	high yield, Mn ion contamination can be avoided, efficient	handling difficulty pollution	2015[62]

https://doi.org/10.1021/acsmaterialsau.1c00022
ACS Mater. Au 2021, 1, 37−54

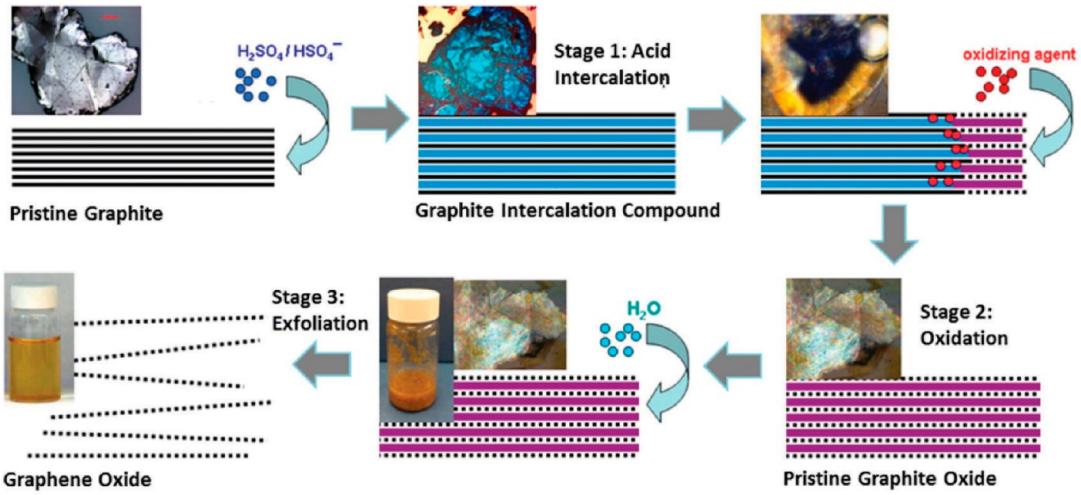

Figure 2. Synthesis diagram of GO from pristine graphite using chemical oxidant method. Reproduced with permission from ref 75. Copyright 2014 American Chemical Society.

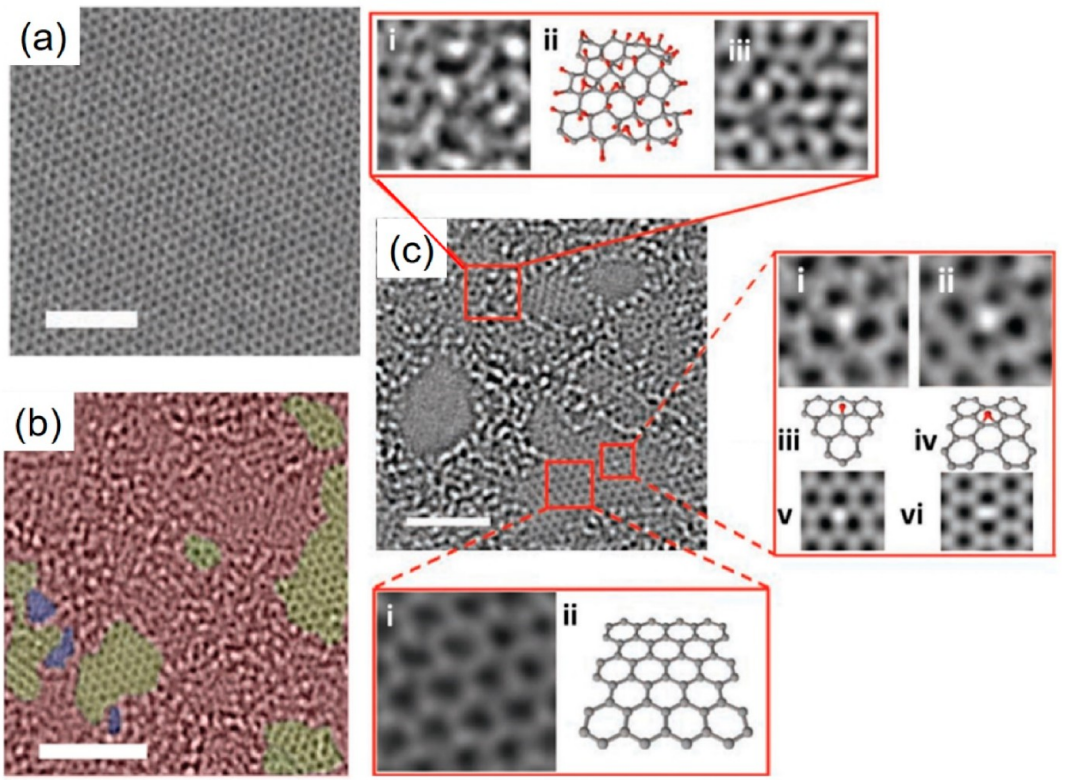

Figure 3. (a) Ultrahigh-resolution TEM image of pristine GR. (b) High-contrast aberration-corrected TEM images of GO. (c) Ultrahigh-resolution TEM image of GO. Reproduced with permission from ref 84. Copyright 2010 Wiley.

2.2. Structure

The chemical composition of GO is analogous to graphite oxide, including aromatic and aliphatic carbon regions, and the ratio of C/O in GO is usually maintained at 1.5 to 2.5.[75,76] However, the precise structure of GO is still controversial because of its nonstoichiometric nature and strong hygroscopic property.[77] Over the past few years, various GO structure models have been presented.[1,61,78] Among these, the most widely accepted is the Lerf–Klinowski model proposed in 1998, which contains epoxy, hydroxyl, and carboxyl groups.[79−81] These oxygen-containing functional groups on the GO surface enable GO to possess benign dispersion and adsorption properties.[1,82] Various spectral techniques have been used to comprehend the electronic structure of GO.[65,83] For example, Erikson et al. have confirmed the Lerf–Klinowski model using the high-resolution transmission electron microscopy (TEM).[84] As displayed in Figure 3a, they have found that the original GR possesses a complete carbon lattice. However, as shown in Figure 3b,c, GO sheets are filled with abundant disordered oxidation regions and defective pores formed after peroxidation of C atoms into CO and CO_2.[48,85] These abundant structural defects on GO surface lead to unsatisfactory electrical conductivity of RGO.[48,86]

https://doi.org/10.1021/acsmaterialsau.1c00022
ACS Mater. Au 2021, 1, 37−54

3. PHOTOCATALYSIS-RELATED PROPERTIES OF GRAPHENE OXIDE

3.1. Electrical Conductivity Properties

Different from GR with superior electrical conductivity, GO is electrically insulated.[3,87] Nevertheless, the conductivity of GO can be distinctly improved by the reduction treatment due to the recovery of graphitic networks of sp^2 bonds during the reduction process.[76,88−90] Stankovich et al. have evaluated the conductivity of raw graphite, GO, and reduced graphene oxide (RGO) with 30% relative humidity.[54] The result indicates that the conductivity of RGO is about 5 orders of magnitude higher than that of GO and about 10 times lower than that of original graphite.[54,77] In addition, thermal, electrochemical, and chemical reduction are frequently used to convert GO into RGO, and thermal reduction techniques generally recover the conductivity of GO more efficiently than chemical reduction methods.[78,91] While most of the oxygenated functional groups of GO can be eliminated by reduction treatment, residual defects lead to inferior conductivity of RGO compared with defect-free GR.[76,92]

3.2. Surface Adsorption Properties

Due to the 2D structure, abundant surface oxygenated functional groups, and high specific surface area, GO is a desired support to increase the adsorption capacity of composite photocatalysts.[1,93] According to the disparate reaction system, the forms of reciprocity between adsorbates (e.g., poisonous metal ions, dyestuff, and organics) and GO are diverse, which include physical, electrostatic, and chemical interaction.[61] As shown in Figure 4, in addition to physical

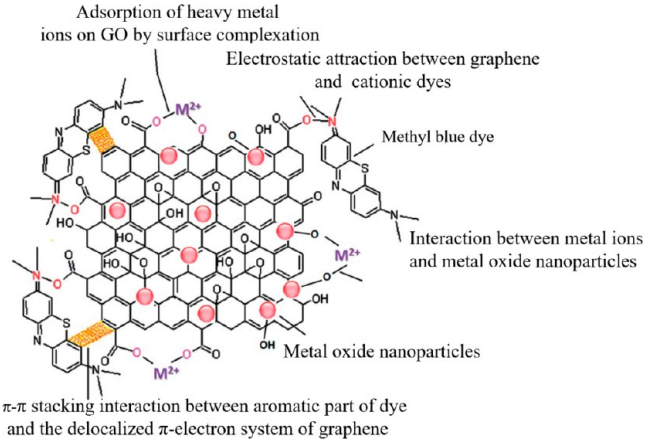

Figure 4. Schematic diagram of various adsorption types between reactants and GO derived hybrid photocatalysts. Reproduced with permission from ref 93. Copyright 2014 Royal Society of Chemistry.

adsorption of target reactants on the surface of GO, the surface oxygen-containing functional groups enables GO to interact with a wide variety of molecules and metal ions.[1] Moreover, the aromatic regions of GO can form a $\pi-\pi$ stacking interaction with organic pollutants containing aromatic structures, thus contributing to improving the adsorption of reaction substrates.[45] The increased adsorption ability contributes to the gathering of the target substrates from the solution to the surface of the photocatalysts.[61,94] As a result, reactants adsorbed on the GO surface can react effectively with the active substances, thus speeding up the photoredox reaction efficiency.[45] Notably, 2D GO with a large π-conjugated structure exhibits excellent adsorption ability for CO_2 molecules, which enables it to be used as a desirable support for photocatalytic CO_2 reduction.[43,95]

3.3. Dispersibility Properties

The dispersibility of GO in solvent mainly depends on the properties of solvent and the functional groups on GO.[96] Owing to the abundant oxygenated functional groups, GO can be dispersed in water and some polar organic solvents, while GO in nonpolar solvents usually exhibits inferior dispersibility (Figure 5).[97,98] However, the dispersibility of GO is not entirely determined by the polarity of the solvent.[99] For example, GO can be effectively dispersed in *N*-methyl pyrrolidone (NMP) but not in dimethyl sulfoxide (DMSO), although DMSO possesses the same net dipole moment with NMP.[98] Another primary assumption is that the surface tension of solvent and GO needs to be matched as much as possible to obtain a minimum free energy of mixing.[31,97] According to the Derjaguin−Landau−Verwey−Overbeek (DLVO) theory, repulsive forces among charged GO sheets are significant for the dispersion and aggregation behavior of GO sheets.[100,101] The zeta potential test results indicate that GO surface is negatively charged, which helps GO to disperse in solution.[102] In addition, the pH is also important for the stability of the GO dispersion. In basic pH conditions, GO can be uniformly dispersed because of the mutual repulsion between GO sheets.[103,104] However, acidic pH conditions lead to obvious aggregation of GO sheets, because the electrostatic repulsion is not enough to counter accumulation under the low pH circumstance.[65,105] Furthermore, the thermodynamic and kinetic behavior of GO sheets in solvents have also been investigated by theoretical calculations, and the results indicate that the intensive hydrogen bonds between deprotonated carboxyl groups and H_2O molecules can enhance the dispersibility of GO.[106,107]

3.4. Semiconductor Properties

The valence band maximum (VBM) and conduction band minimum (CBM) of GR composed of bonding π and antibonding π (π^*) orbitals, respectively, contact at the Brillouin zone corners, making the monolithic GR a zero-bandgap semiconductor.[61,108,109] The close C−C distance results in dense overlap of electron bands, and the behavior of electrons and holes in the GR is similar to that of mass-free charges.[40,110] As discussed above, GO is covalently embellished with oxygenated functional groups, and these C−O bonds in GO destroy the expanded sp^2 conjugated network, which leads to the transform of zero-gap GR to semiconductor GO.[111,112] The CBM of GO consists of the antibonding π^*-orbital and the VBM consists of the O 2p orbital, rather than the π-orbital.[113,114] In addition, the band gap of GO gradually decreases from 3.5 to 1 eV accompanied by the elevated C/O ratio.[115,116] GO with oxygen-containing functional groups can be considered as a p-type semiconductor, and GO can be transformed from p-type to n-type semiconductor by substituting oxygen-containing groups with nitrogen-rich groups.[114,117]

4. MULTIFARIOUS ROLES OF GRAPHENE OXIDE IN PHOTOCATALYSIS

4.1. Precursor of Reduced Graphene Oxide

The most diffusely accepted role of GO is considered to the precursor of RGO.[83,118−121] Table 2 shows a series of typical

https://doi.org/10.1021/acsmaterialsau.1c00022
ACS Mater. Au 2021, 1, 37−54

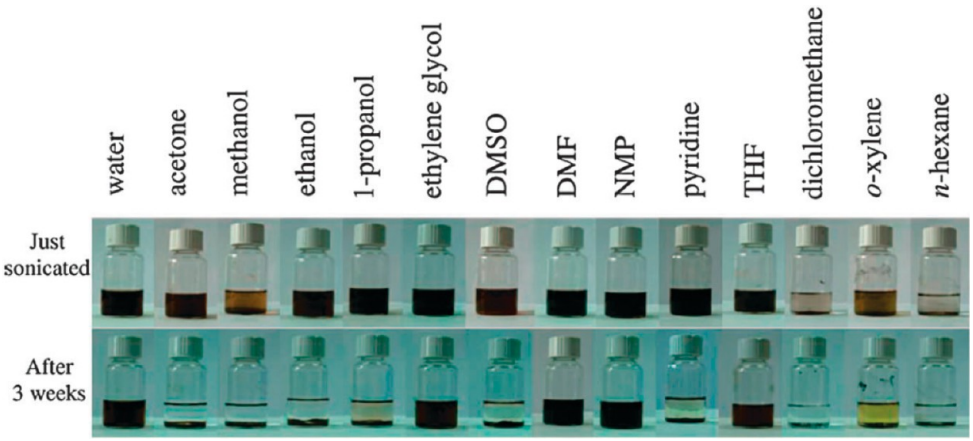

Figure 5. Images of GO dispersed in water and various organic solvents. Reproduced with permission from ref 98. Copyright 2010 American Chemical Society.

Table 2. Various Photocatalytic Applications over RGO-Based Composites

composite photocatalyst	photocatalytic applications	light source	photocatalytic activity enhancement	ref
TiO_2 nanotube array-RGO	degradation of methyl blue (MB)	visible light xenon lamp	1.6-fold of blank TiO_2	128
ZnO-RGO	degradation of MB	UV light xenon lamp	1.3-fold of bare ZnO	129
TiO_2-RGO	photoinactivation of *Escherichia coli* bacteria	solar light	7.5-fold of blank TiO_2	130
AgInZnS-RGO	H_2 evolution form H_2O splitting	visible light xenon lamp	2-fold of blank AgInZnS	131
ZnS-RGO	H_2 evolution form H_2O splitting	visible light xenon lamp	8-fold of blank ZnS	132
$ZnIn_2S_4$ nanosheets-RGO	H_2 evolution form H_2O splitting	visible light xenon lamp	4-fold of blank $ZnIn_2S_4$ nanosheets	133
CdS-RGO	H_2 evolution form H_2O splitting	visible light xenon lamp	2-fold of bare ZnS	134
$Zn_{0.5}Cd_{0.5}S$ nanorods- RGO	H_2 evolution form H_2O splitting	visible light xenon lamp	2-fold of bare $Zn_{0.5}Cd_{0.5}S$ nanorods	135
TiO_2-RGO	CO_2 reduction into CH_4	UV light xenon lamp	2-fold of blank TiO_2	127
CdS nanorod-RGO	CO_2 reduction into CH_4	visible light xenon lamp	10-fold of blank CdS nanorod	136
Cu_2O-RGO	CO_2 reduction into CO	visible light xenon lamp	6-fold of blank Cu_2O	137

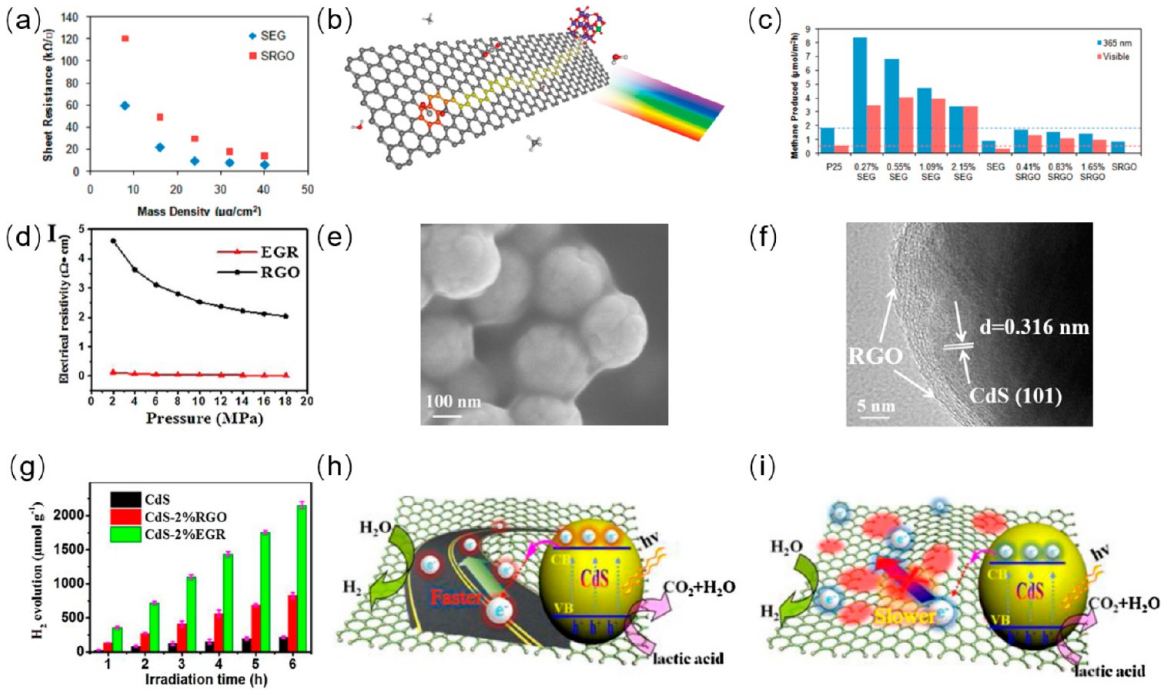

Figure 6. (a) Resistances of SEG and SRGO. (b) Schematic illustration of photocatalytic CO_2 reduction over SEG-TiO_2 hybrid. (c) Photocatalytic H_2 evolution rates over SEG-P25 and SRGO-P25 hybrid. Reproduced with permission from ref 127. Copyright 2011 American Chemical Society. (d) Resistances of RGO and EGR. (e) Typical SEM image of CdS-2%RGO composite. (f) TEM image of CdS-2%RGO composite. (g) Time-online photoactivity over CdS, CdS-2%RGO and CdS-2%EGR hybrids. Diagram of H_2 evolution over (h) CdS-EGR and (i) CdS-RGO hybrids. Reproduced with permission from ref 124. Copyright 2018 Elsevier.

https://doi.org/10.1021/acsmaterialsau.1c00022
ACS Mater. Au 2021, 1, 37−54

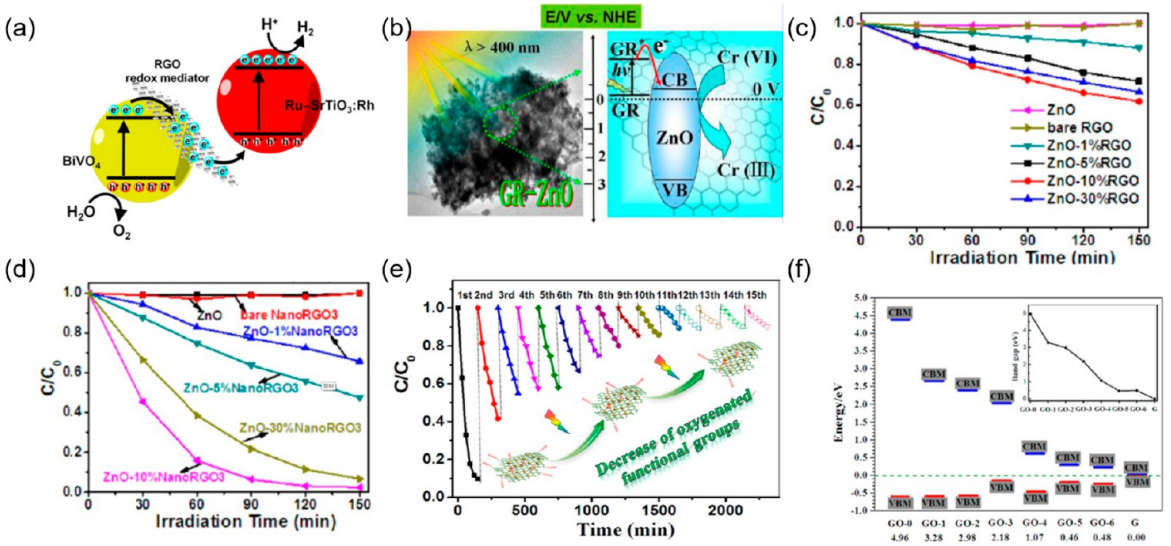

Figure 7. (a) Diagram of Z-scheme system. Reproduced with permission from ref 138. Copyright 2011 American Chemical Society. (b) Diagram of photosensitive mechanism of RGO in the GR-ZnO composite system. Reproduced with permission from ref 141. Copyright 2013 American Chemical Society. Photocatalytic performance of (c) ZnO-RGO and (d) ZnO-NanoRGO3 for the reduction of Cr(VI). (e) Recycled testing of ZnO-10%NanoRGO3. (f) Theoretical calculation results over VBM, CBM and bandgaps of graphene with diverse content of oxygen-containing functional groups. Reproduced with permission from ref 142. Copyright 2016 American Chemical Society.

GO derived RGO-based composites for various photocatalytic applications. After introduction of RGO, the photocatalytic activity of these composites has an improvement, which is mainly because RGO can act as an electron conductor to promote the migration of the photogenerated charge carriers.[122] In 2010, Xu et al. argued that TiO_2−RGO composite photocatalysts are in essence the same as other TiO_2−carbon (carbon nanotubes, fullerenes, and activated carbon) counterparts with regard to enhancing the photoactivity of TiO_2.[123] The key features for the prepared TiO_2-RGO composites, including the increased adsorptivity of pollutants, enhanced light absorption intensity and extended light absorption range, and promoted charge separation and transportation, can also be observed in their counterparts of TiO_2−CNT prepared via the same approach.[3] Therefore, they emphasize that researchers need to give more effort to exploring how to rationally utilize intriguing characteristics of RGO. The conductivity of the RGO is greatly reduced by the abundant surface defects.[124,125] In this regard, the synthesis of solvent exfoliated graphene (SEG) with decreased defects has been developed.[3,126] For example, Hersam et al. have reported a comparative research between SEG-P25 and SRGO-P25 hybrid.[127] The Raman spectra indicate that the defect density of SEG is much lower than that of SRGO. In addition, the conductivity of SEG is obviously higher than that of SRGO (Figure 6a). The increased conductivity of SEG indicates a longer electronic mean free path, which accelerates the migration of photoinduced charge carriers (Figure 6b). Therefore, SEG-TiO_2 hybrids exhibit superior photocatalytic performance compared with SRGO-TiO_2 composites (Figure 6c). In addition, Xu et al. have used the defect-few, commercial Elicarb graphene (EGR) to prepare EGR-CdS hybrid.[124] As shown in Figure 6d, EGR shows significantly higher conductivity than RGO. To resolve the poor dispersion defect of EGR, sodium dodecyl benzene acid (SDBS) has been used to modify EGR with negatively charged hydrophilic functional groups. As shown in Figure 6e,f, the positively charged CdS nanospheres can be compounded with EGR by an electrostatic self-assembly strategy. Under the same conditions, CdS-EGR composite exhibits better performance than CdS-RGO composite for photocatalytic H_2 evolution, which is due to the fact that superior conductivity of EGR can guarantee the more efficient transfer of photoinduced electrons of CdS (Figure 6g−i).

Furthermore, Amal et al. have indicated that RGO can act as an electronic medium in a Z-scheme photocatalytic system.[138] In this system, $BiVO_4$ has been selected as the O_2-generating photocatalyst, and Ru-$SrTiO_3$:Rh has been used as the H_2-generating photocatalyst. As shown in Figure 7a, the electrons are first migrated from $BiVO_4$ to RGO, and then these accumulated electrons on RGO are combined with holes on Ru-$SrTiO_3$:Rh. Besides being a photoelectron mediator and acceptor, GO-derived RGO can also be used as a photosensitizer. Du et al. have utilized theoretical calculations to research the interfacial interaction of the RGO-TiO_2 composite, and the result indicates that electrons on RGO will transfer to TiO_2 under visible light illumination.[139] Xu et al. have provided direct experimental evidence to prove the photosensitizers role of RGO by designing RGO-ZnS and RGO-ZnO systems (Figure 7b).[140,141] Moreover, Xu et al. have also indicated that photosensitive efficiency of RGO can be improved by further oxidation of the GO.[142] Further oxidation reduces the size of GO sheets and increases the content of oxygen-containing functional groups (the resulting samples are called Nano GO). Using GO and NanoGO as precursors, ZnO-RGO and ZnONanoRGO hybrids with similar structure have been synthesized. The photocatalytic activity test over ZnO-RGO and ZnO-NanoRGO composite indicates that NanoRGO shows remarkably higher photosensitive efficiency than RGO (Figure 7c,d). In addition, controlled experiments and cycle tests manifest that the presence of residual oxygen-containing functional groups is the primary factor determining the photosensitive performance of RGO (Figure 7e). The theoretical calculation indicates that residual oxygenated functional groups on RGO surface have a vital effect on its band gap. With the increase of residual

https://doi.org/10.1021/acsmaterialsau.1c00022
ACS Mater. Au 2021, 1, 37−54

oxygen-containing functional groups, the band gap of RGO widens with the upshift of CB, which improves the reduction ability of electrons and enhances the photosensitive efficiency of RGO (Figure 7f).

4.2. Cross-Linked Framework for Constructing an Aerogel Photocatalyst

Traditional RGO-based powder photocatalysts are easily stacked, resulting in failure to make full use of intrinsic properties of RGO.[45] In addition, the recycling of the powder photocatalyst not only requires complex operation, but also, a large number of lost photocatalysts in this process may endanger human health and pollute the environment.[61,143] Moreover, agitation is always an unavoidable process to disperse powder photocatalysts. However, this powerful mechanical stirring treatment is not in line with practical applications.[144] Constructing macroscopic 3D GR aerogels-based photocatalysts using GO as a cross-linked framework has been considered as a promising method to avoid above issues.[145,146] In addition, the macroblock structure of GR aerogels-based photocatalysts allows them to be easily separated from aqueous solutions.[147] Because GR aerogels are lightweight, they can be suspended in an aqueous solution to ensure effective absorption of sunlight and contact with reactant molecules in practical application.[148] Furthermore, GR aerogels possess other special advantages besides the characteristics of powder GR sheets.[86] On the one hand, the 3D network-like structures can offer multidimensional electron transport routes, which contribute to the valid migration of photoinduced electrons. On the other hand, hierarchically porous structures of GR aerogel can increase specific surface area, thus promoting the effective adsorption of reactants.[149,150] Adding cross-linking agents to a GO solution is a simple and efficient method to prepare 3D GO aerogels, and commonly used cross-linking agents include polymers, small organic molecules, biomolecules, and multivalent ions.[151] Shi et al. have reported the assembly of GO sheets by adding poly(vinyl alcohol) (PVA) as a cross-linker to induce the formation of a 3D GO hydrogel.[152] During the synthesis process, the hydrogen bonding interaction between hydroxyl-rich PVA chains and oxygen-containing functional groups on GO sheets accounts for forming the cross-linking sites.[151] In addition, hydrothermal reduction of GO is an effective method to construct GR aerogels-based photocatalysts.[145,153] A suitable reduction temperature is usually necessary, and the temperatures usually need to be above 150 °C.[151,154] For example, Shi et al. have prepared the GR aerogels through hydrothermal reduction of GO at 180 °C for 12 h (Figure 8a).[155] As presented in Figure 8b–d, the prepared GR aerogels possess excellent mechanical strength and abundant pore structure.

Moreover, Wang et al. have reported the synthesis of carbon quantum dots/GR aerogel (CQDs/GA) hybrids via hydrothermal reduction method.[156] As shown in Figure 9a, carbon quantum dots (CQDs) can be well dispersed in aqueous solution and effectively adsorbed on the GO surface by $\pi-\pi$ interaction. Hydrothermal reduction leads to the removal of hydrophilic groups of GO, resulting in cross-linking of GO hydrophobic regions. Meanwhile, the residual hydrophilic oxygen-containing groups of GO can adsorb a H_2O molecule by hydrogen bonding, which hinders the parallel stacking of GR nanosheets, thus forming the 3D GR hydrogel structure. The final 3D CQDs/GR aerogel composites can be obtained by freeze-drying the CQDs/GR hydrogel. As shown in Figure 9b, electrons in the VB of CQD are excited to the CB and then migrate to the surface of 3D GR aerogel through a multidimensional electron transfer pathway, including 2D GR nanosheets and 3D cross-linking framework, which can effectively promote the reduction of Cr (VI) to nontoxic Cr (III).

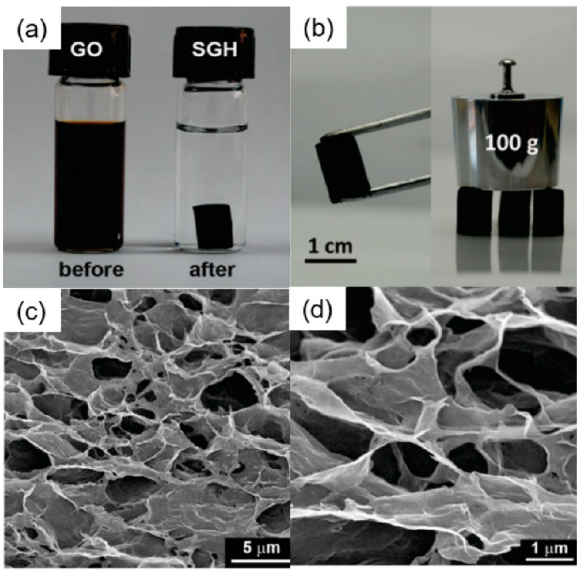

Figure 8. (a) Picture of GO dispersion before and after hydrothermal reduction. (b) Picture of 3D GR aerogel. (c, d) SEM images of 3D GR aerogel. Reproduced with permission from ref 155. Copyright 2010 American Chemical Society.

Except for the hydrothermal reduction method, chemical reduction can also be used to construct 3D GR aerogel photocatalysts. Chen et al. have indicated that the reduction time required to synthesize GR aerogel is disparate for diverse reductive agents.[157] Furthermore, they have also indicated that the shape of the 3D GR hydrogels prepared by chemical reduction method can be regulated by changing the shapes of the reactors. Xu et al. have synthesized RGO-$Ti_3C_2T_x$-Eosin Y (RTiC/EY) hydrogel using $NaHSO_3$ as reducing agent.[158] As shown in Figure 10a, $Ti_3C_2T_x$, EY, $NaHSO_3$, and GO are first mixed to obtain a colloid solution, and then the mixed colloids react at 70° to form RTiC/EY hydrogels. The RTiC/EY aerogel can be obtained after freeze-drying the RTiC/EY hydrogel, and the RTiC/EY aerogel presents a porous structure with thin pore walls (Figure 10b). As displayed in Figure 10c,d, under the same conditions, the RTiC/EY aerogel has showed obviously better performance than the RTiC/EY powder in reduction of Cr (VI) and photocatalytic hydrogenation of 4-nitroaniline (4-NA). As schematically illustrated in Figure 10e, there are two main reasons for the elevated photocatalytic performance of RTiC/EY aerogels. First, the porous structure of the RTiC/EY aerogel endows them to possess multidimensional electron migration route, which accelerates the transfer of electrons from EY. In addition, the increased surface area of RTiC/EY aerogels can promote the adsorption of reactants.

4.3. Macromolecular Surfactant

A large number of hydrophilic oxygenated functional groups make GO possess excellent water solubility.[48,159] In addition, aromatic regions of GO can provide effective sites for interaction with some insoluble substances by $\pi-\pi$ inter-

https://doi.org/10.1021/acsmaterialsau.1c00022
ACS Mater. Au 2021, 1, 37–54

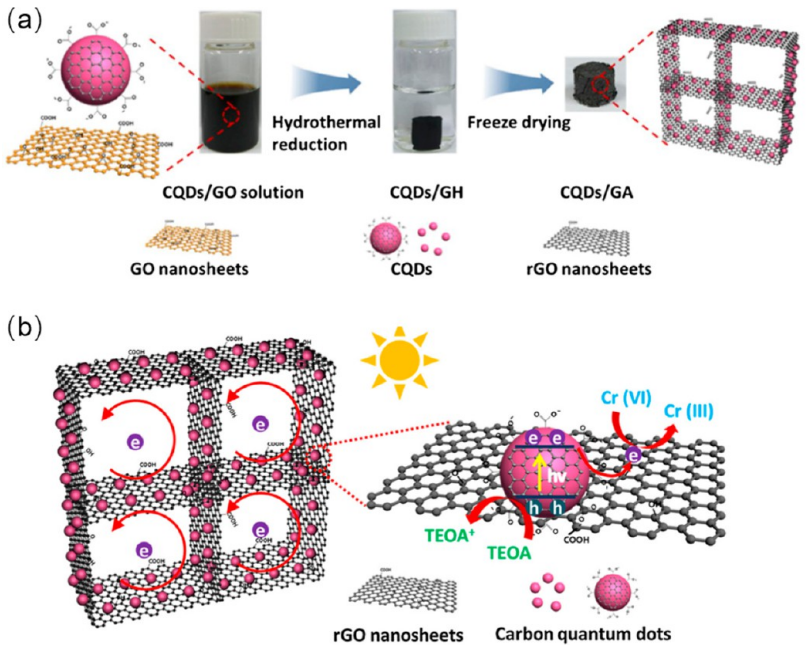

Figure 9. (a) Synthesis schematic of the 3D CQDs/GA hybrid. (b) Diagram of the reaction mechanism over 3D CQDs/GA hybrids. Reproduced with permission from ref 156. Copyright 2018 Elsevier.

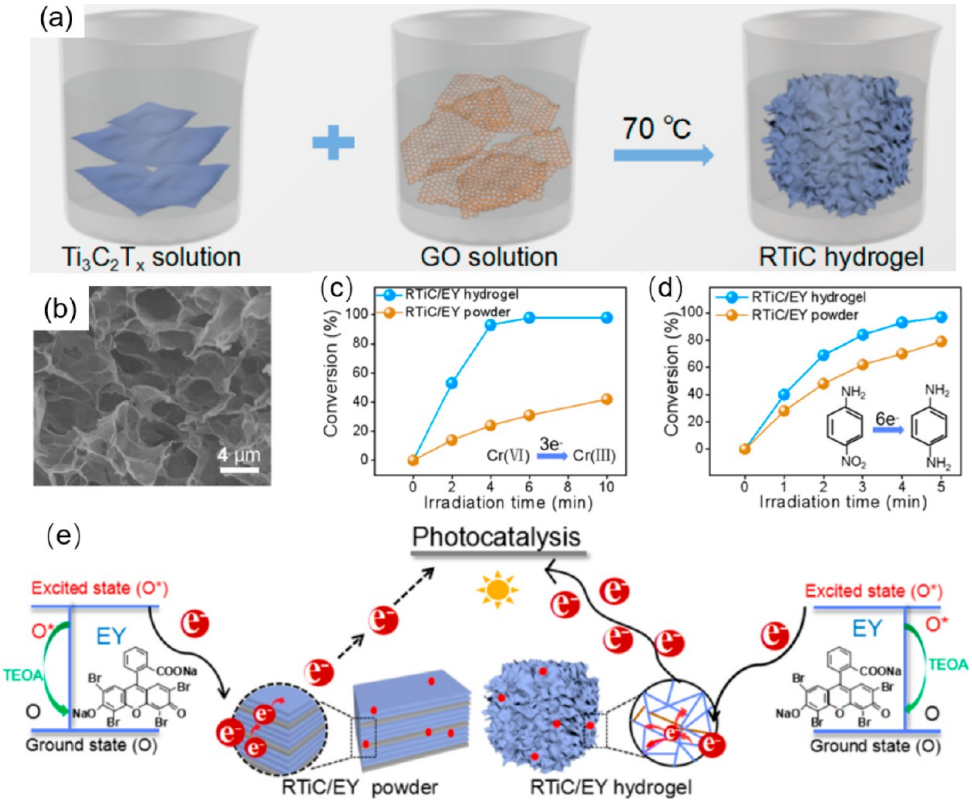

Figure 10. (a) Preparation diagram of RTiC hydrogel. (b) SEM image of RTiC aerogel. (c, d) Results of photocatalytic activity test over RTiC/EY hydrogel and RTiC/EY powder. (e) Schematic diagram of photocatalytic reaction mechanism. Reproduced with permission from ref 158. Copyright 2019 American Chemical Society.

actions.[83,160] As a result, the unique structural properties of GO enable it to be a promising "macromolecular surfactant". Huang et al. have demonstrated that GO as surfactants can be used to disperse single-walled carbon nanotubes (SWCNTs).[31,99] As shown in Figure 11a,b, SWCNTs cannot be well dispersed in water, and the SEM image shows the stacked structure of SWCNTs. However, when SWCNTs have been fully sonicated in GO solution, SWCNTs can be effectively dispersed, and the SEM image reveals that the SWCNTs are disentangled and highly dispersed (Figure 11c).[161] Furthermore, Xu et al. have also reported that GO can be used as a surfactant to disperse commercial EGR and

https://doi.org/10.1021/acsmaterialsau.1c00022
ACS Mater. Au 2021, 1, 37−54

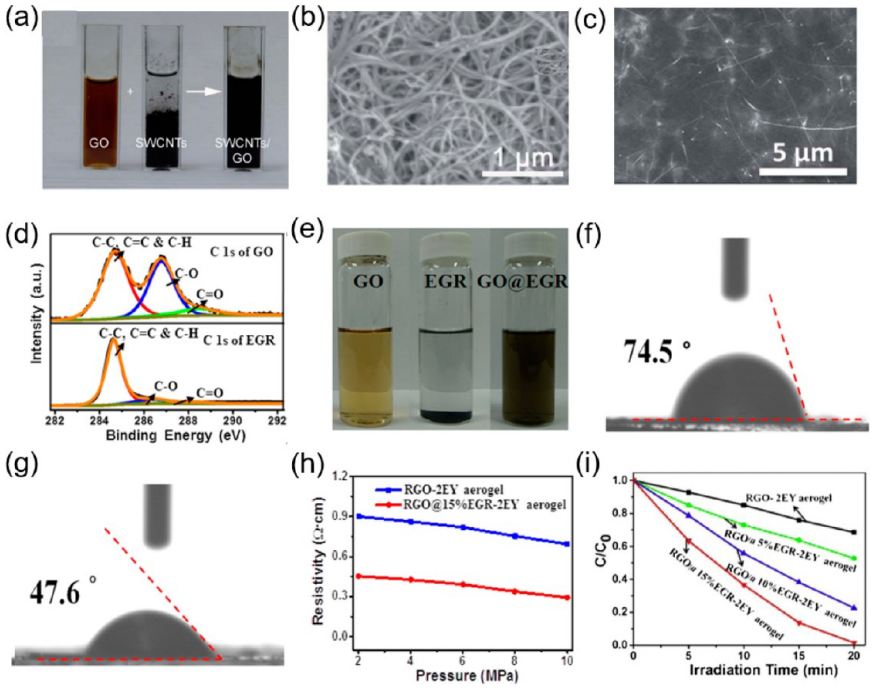

Figure 11. (a) Pictures of GO, SWCNTs, and SWCNTs/GO dispersed in water. SEM images of SWCNTs (b) before and (c) after sonication with GO. Reproduced with permission from ref 161. Copyright 2012 Royal Society of Chemistry. (d) C 1s XPS spectra of GO and EGR. (e) Pictures of GO, EGR, and GO@EGR dispersed in water. Contact angle measurement for (f) EGR and (g) GO@EGR. (h) Resistivity−pressure (R−P) curves of obtained samples. (i) Photocatalytic reduction of Cr(VI) over different samples. Reproduced with permission from ref 102 Copyright 2010 Elsevier.

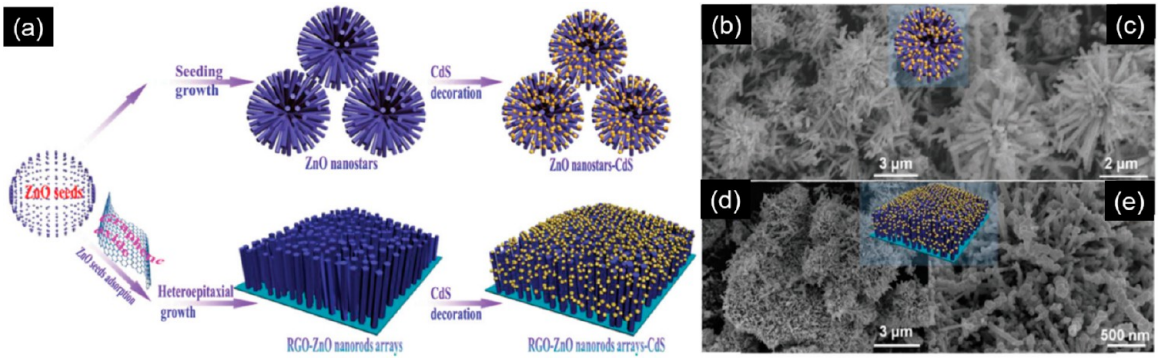

Figure 12. (a) Preparation diagram of ZnO-CdS and RGO-ZnO-CdS hybrids. SEM images of (b, c) ZnO-CdS and (d, e) RGO-ZnO-CdS hybrids. Reproduced with permission from ref 170. Copyright 2015 Wiley.

provides basic framework for constructing 3D RGO@EGR-Eosin Y (RGO@EGR-EY) aerogel.[102] As shown in Figure 11d, C 1s X-ray photoelectron spectroscopy (XPS) of GO and EGR indicates that GO possesses abundant oxygenated functional groups, while the EGR surface lacks oxygenated functional groups. After the hydrophobic EGR powders are fully sonicated in GO solution, the GO@EGR suspension can remain stable even after two months of deposition (Figure 11e). Moreover, as shown in Figure 11f,g, the contact angle of the GO@EGR film is smaller than that of the EGR membrane, which indicates that GO as surfactant can effectively improve the hydrophilicity of EGR. Figure 11h presents the resistivity of obtained samples, and the result shows that the conductivity of RGO@15%EGR-2EY aerogel is significantly higher than that of RGO-2EY aerogel. The enhanced conductivity of RGO@15%EGR-2EY aerogel promotes the migration of photoinduced charge carriers between the RGO@15%EGR aerogel and EY, thus boosting the photocatalytic performance of RGO@15%EGR-2EY aerogel (Figure 11i).

In addition to dispersing insoluble carbon materials, GO can also be used as surfactants to induce the synthesis of semiconductor and metal composites. For example, Yao et al. have used GO as surfactant to construct flower-like ZnO, and GO can induce the synthesis of flower-like ZnO more effectively than classical surfactants, such as dodecyl trimethylammonium bromide (CTAB) and dodecyl sweet methyl base.[162] Furthermore, Pan et al. have indicated that GO as a macromolecular surfactant can be used to regulate morphology and induce oxygen vacancy formation in ZnO.[163] Notably, RGO cannot act as a macromolecular surfactant like GO, indicating that the morphology regulation of ZnO is primarily attributed to the oxygenated functional groups on GO surfaces. Furthermore, Zhang et al. have also indicated

https://doi.org/10.1021/acsmaterialsau.1c00022
ACS Mater. Au 2021, 1, 37−54

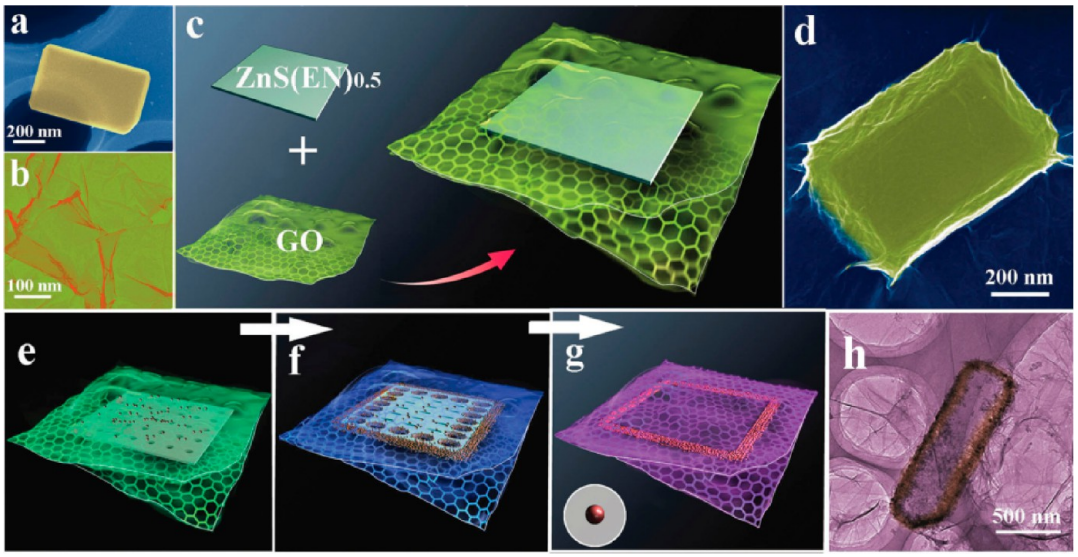

Figure 13. (a, b) SEM images of $ZnS(EN)_{0.5}$ NS and GO. (c, d) Diagram of a $ZnS(EN)_{0.5}$ NS wrapped in GO sheets. (e–g) Synthetic diagram of ZnS-NF@RGO. (h) TEM image of the ZnS-NF@RGO. Reproduced with permission from ref 172. Copyright 2015 Wiley.

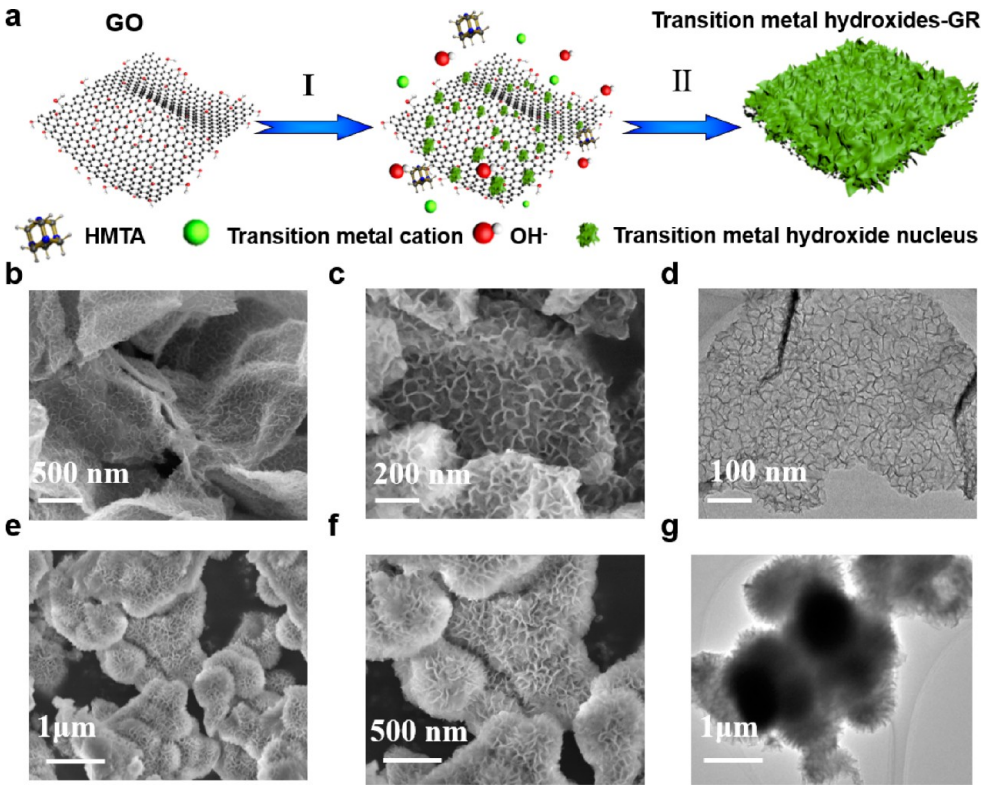

Figure 14. (a) Synthesis diagram of transition metal hydroxides-GR composites. (b, c) SEM images of $Ni(OH)_2$-10%GR. (d) TEM image of $Ni(OH)_2$-10%GR. (e, f) SEM images of bare $Ni(OH)_2$. (g) TEM image of bare $Ni(OH)_2$. Reproduced with permission from ref 95. Copyright 2020 Springer Nature.

that GO can act as surfactant to facilitate the preparation of a stable Au–Pd alloy.[164]

4.4. Two-Dimensional Growth Template

The unique 2D structure and amenable wet-chemistry processability of GO enable it to be used as a versatile template for the construction of nanomaterials with various morphologies.[44,165] Notably, GO can be simply eliminated by calcination in air, thus avoiding the utilization of harmful acids/base.[166,167] Furthermore, in some situations, a GO template can also be directly used to promote the electron transfer in the photocatalytic system, which not only avoids additional removal process but also enhances the photocatalytic activity of composites.[168] Up to now, a variety of composite photocatalysts with specific morphologies have been prepared by using GO as 2D growth template.[44,169] For example, Han et al. have used GO as a 2D growth template for *in situ* growth of 1D ZnO nanorod and the synthesis of RGO-ZnO-CdS ternary composites using CdS as photosensitizer

https://doi.org/10.1021/acsmaterialsau.1c00022
ACS Mater. Au 2021, 1, 37–54

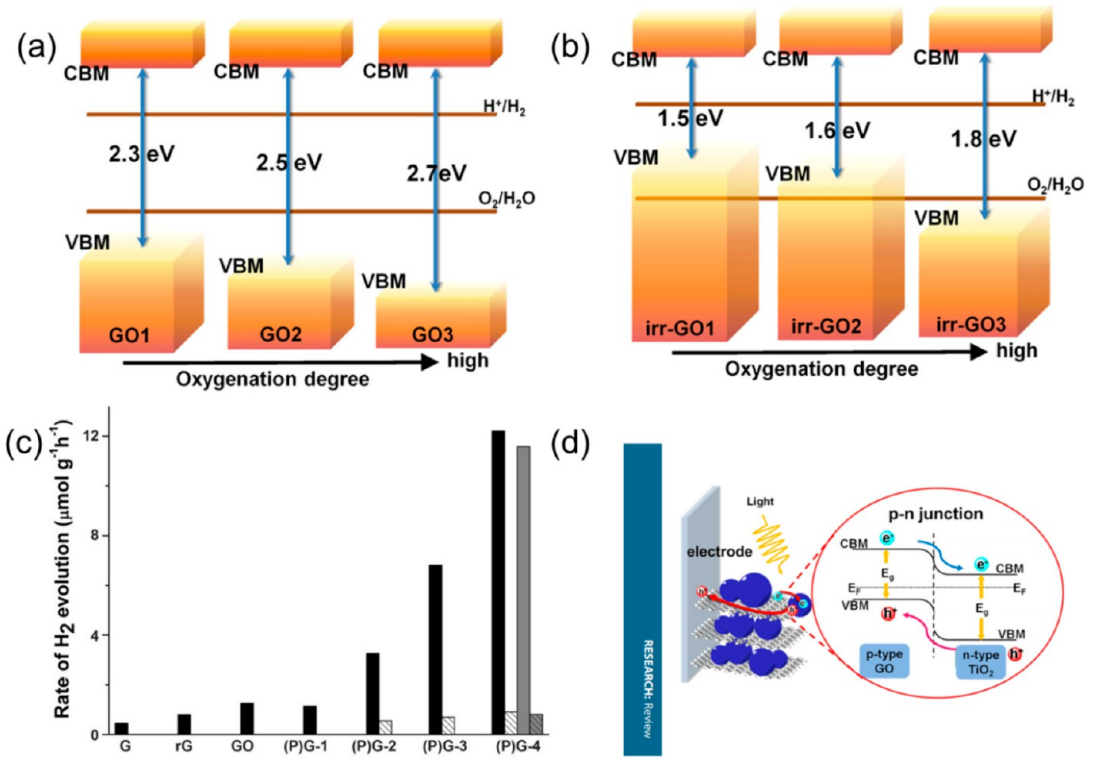

Figure 15. Energy level diagrams of (a) GO and (b) irr-GO. Reproduced with permission ref 40. Copyright 2011 American Chemical Society. (c) H_2 evolution rates of GO and P-GO. Reproduced with permission from ref 175. Copyright 2013 Wiley. (d) Diagram of p−n heterojunction formed at the interface between GO and TO_2. Reproduced with permission ref 177. Copyright 2015 American Chemical Society.

(Figure 12a).[170] As displayed in Figure 12b−e, the blank ZnO presents a stacked star-like morphology, but when GO has been used as growth templates, the ZnO-RGO composite shows a uniform nanorod array morphology. Abundant oxygenated functional groups of GO can serve as effective sites for anchoring ZnO seeds, as well as induce the heteroepitaxial growth of ZnO nanorod array.

Especially, GO as 2D growth templates have unique advantages in inducing synthesis of 2D composites materials.[25,61] For instance, Liu et al. have prepared a series of 2D porous metal oxide by using GO as growth templates.[171] Zhao et al. have synthesized 2D ZnS nanoframe (NF)@GO composites using 2D GO as growth templates.[172] As shown in Figure 13a−c, the ZnS-ethylenediamine ($ZnS(EN)_{0.5}$) nanosheets are selected as the precursors of the ZnS NF, and $ZnS(EN)_{0.5}$ nanosheets are primarily wrapped by GO to form an envelope-like quasi-2D space. The evolution of the $ZnS(EN)_{0.5}$ sheets is confined within the quasi-2D space, which efficiently protects the side edges of $ZnS(EN)_{0.5}$ sheets from collapse and facilitates the migration of Zn^{2+} and S^{2-} ions from interiors to the side edges of the $ZnS(EN)_{0.5}$ sheets (Figure 13d−g). Therefore, $ZnS(EN)_{0.5}$ sheets can be gradually transformed into ZnS NFs assembled on RGO, as presented in Figure 13h.

Furthermore, abundant oxygenated functional groups make GO negatively charged and can be used as an effective template for electrostatic self-assembly with positively charged materials. Chen et al. have reported electrostatic self-assembly of uniform CdS nanospheres (NSPs) with negatively charged GO to synthesize CdS NSPs/RGO composite.[173] Furthermore, Xu et al. have reported the preparation of different transition metal hydroxides nanosheet arrays onto 2D platform of GO.[95] As shown in Figure 14a, after transition metal precursors are added into GO solution, the electrostatic interaction between GO and transition metal cations results in an intimate adsorption of transition metal cations on the surface of GO. Therefore, GO as growth template can induce the heteronucleation and directional crystal growth of transition metal hydroxides in solution phase. As shown in Figure 14b−d, SEM images of $Ni(OH)_2$-10%GR show that a $Ni(OH)_2$ nanosheet array can be uniformly grown on the surface of GO templates. However, without GO as the growth template, the prepared bare $Ni(OH)_2$ presents a sphere-like aggregated structure, which is because nuclear formation and crystal growth of bare $Ni(OH)_2$ lack steric hindrance, thereby resulting in an omnidirectional and superimposed assembly (Figure 14e−g).

4.5. Photocatalyst

Apart from GR-semiconductor composite photocatalysts as discussed above, individual GO can also act as a photocatalyst, because GO with suitable oxidation degree exhibits semiconductor properties.[1,40] For instance, Teng et al. have indicated GO with band gap of 2.4−4.3 eV can be utilized as photocatalysts to produce H_2 from water splitting.[113,114] As presented in Figure 15a, the band gap of GO increases with the elevated oxidation degree, and VBM or CBM of GO1, GO2 and GO3 are suitable for O_2 and H_2 evolution. Nevertheless, in the actual photocatalytic activity test, only the GO3 with the highest degree of oxidation can produce O_2, while GO1 and GO2 cannot produce O_2, which is because the VBM position of GO will change after irradiation, and only irradiated GO3 (irr-GO3) has a sufficiently positive VBM for water oxidation (Figure 15b)

https://doi.org/10.1021/acsmaterialsau.1c00022
ACS Mater. Au 2021, 1, 37−54

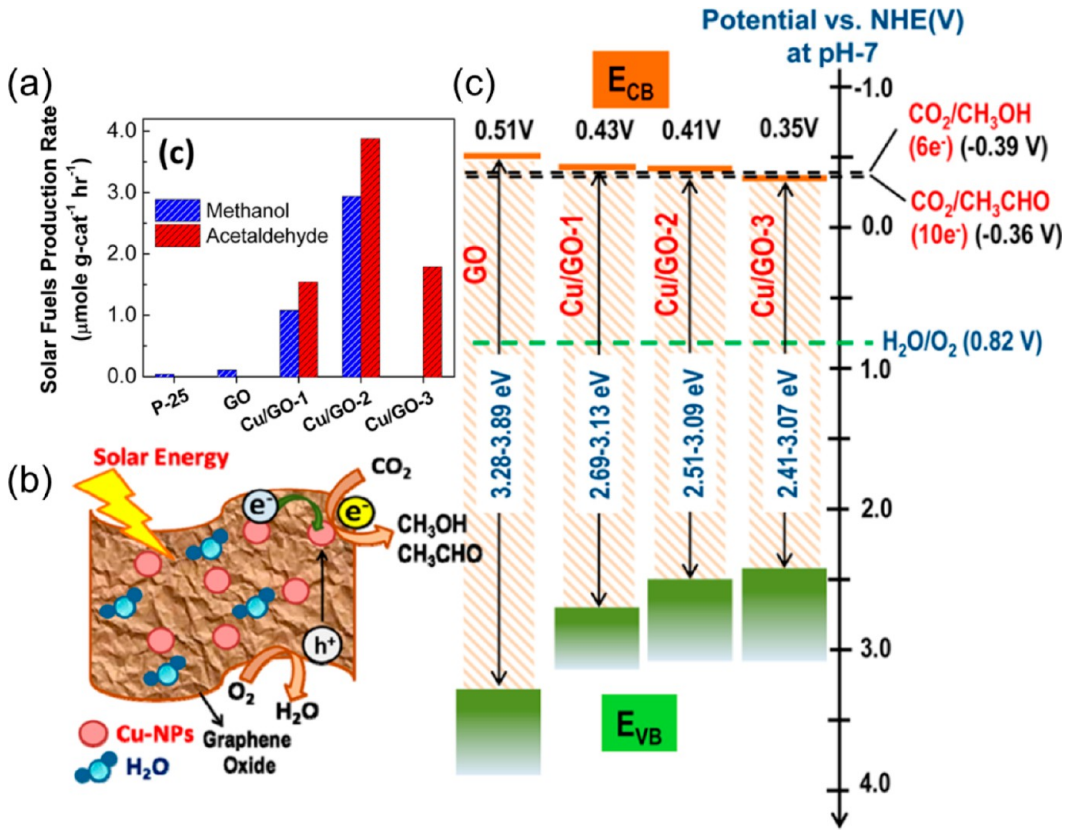

Figure 16. (a) Product generation rates over P25, GO, and Cu/GO. (b) Diagram of photocatalytic CO_2 reduction mechanism over Cu/GO. (c) Energy band structure of GO and Cu/CO composites. Reprinted with permission from ref 181. Copyright 2014 American Chemical Society.

The introduction of cocatalysts is a simple and effective way to optimize performance of GO.[76,174] Agegnehu et al. have reported that deposition of Ni and NiO cocatalysts on GO can boost the performance of GO for photocatalytic H_2 evolution form H_2O splitting.[76] Compared with bare GO, the H_2 evolution rates of NiO-GO and Ni-GO hybrid have increased by about 4 and 7 times, respectively. Heteroatom doping of GO is another efficient way to enhance the performance of GO. For example, Marcos-Sánchez et al. have synthesized P-doped GO (P-GO) and found the H_2 generation rate of P-GO is obviously higher than that of GO (Figure 15c).[175] In addition, similar phenomena can also be seen in the N-doped GO (N-GO) as reported by Garcia-Sánchez et al.[176] Furthermore, GO with a large number of oxygen-containing functional groups can be considered as a p-type semiconductor, and Chen et al. have indicated that p-type GO with n-type TiO_2 can form p−n heterojunction, which contributes to the efficient separation of photoinduced electron−hole pairs (Figure 15d).[177]

GO can be utilized not only as a photocatalyst for H_2 production but also as a photocatalyst for CO_2 reduction to produce useful fuels.[178,179] Chen et al. have reported that GO as a photocatalyst can drive the conversion of CO_2 to methanol, and the photocatalytic performance of GO is obviously better than that of P25.[180] Furthermore, they have also prepared a series of Cu cocatalyst decorated GO (Cu/GO) composites by a one-step microwave method.[181] As displayed in Figure 16a, the generation rate of methanol and acetaldehyde over the optimal Cu/GO-2 (10% Cu) hybrid is distinctly higher than that of GO. The superior photocatalytic performance of the Cu/GO-2 hybrid compared with GO is mainly due to the fact that introduction of Cu cocatalyst can promote the separation of photoinduced electron−hole pairs in GO (Figure 16b). In addition, Cu/GO hybrids with disparate Cu cocatalyst contents possess different energy band structures. As shown in Figure 16c, CBM of Cu/GO-1 (5% Cu) and Cu/GO-2 is viable for the conversion of CO_2 to methanol and acetaldehyde. However, the CBM of Cu/GO-3 (15% Cu) is lower than the CO_2/CH_3OH reduction potential, which results in the disappearance of methanol in product.

5. CONCLUSIONS AND PERSPECTIVES

In this Review, the synthesis, structural, photocatalysis-related properties, and roles of GO in photocatalysis have been summarized. In addition to acting as precursor to synthesize GR, GO can also act as a cross-linked framework for constructing an aerogel photocatalyst, a macromolecular surfactant to disperse insoluble materials, a 2D growth template, and a photocatalyst by itself. Inspired by the current developments described above, some challenges and opportunities for further advancement in this research field are presented as follows:

First, a large number of strong acids and oxidants are inevitably used for current GO synthesis, which causes serious environmental pollution and operational safety problems. In addition, the dispersibility, conductivity, and adsorption property of GO are mainly determined by its size, layer number, and degree of oxidation. However, the GO prepared by existing methods is usually inhomogeneous, leading to an obvious uncertainty in the structure−property correlation. Therefore, more efforts need to be paid to develop environmentally friendly methods for uniform GO preparation.

https://doi.org/10.1021/acsmaterialsau.1c00022
ACS Mater. Au 2021, 1, 37−54

Second, the electrical conductivity of GO-derived RGO has been remarkably decreased because of the residual oxygen-containing functional groups and a large number of defects in RGO. Improving the electrical conductivity of RGO is a direction that needs persistent endeavor in the future. In this regard, efficient reduction methods need to be developed to reduce the residual oxygenated functional groups and restore π-conjugation of RGO as much as possible. In addition, heteroatom doping of RGO is also a promising way to improve the electrical conductivity of RGO.

Third, there are still many issues that need to be solved for further development. For example, a convincing explanation is still absent for the semiconductor character of GO. Besides, the exact structure of GO has also not been confirmed. Hence, more in-depth systemic investigations for these issues from both theoretical and experimental aspects are highly desirable. Notably, rapidly developed *in situ* characterization techniques allow real-time detection of changes in the atomic structure of the photocatalyst, which will help to understand the semiconductor properties of GO and accurately elucidate structural characteristics of GO.

Fourth, the current applications of GO-derived composites mainly focus on photocatalytic degradation pollutants and H_2 evolution from water splitting. Applications in photoreduction of CO_2 and atmospheric ammonia synthesis need further exploration. Furthermore, most current photocatalytic reactions require the addition of sacrificial agents, which not only significantly augments the reaction cost but also squanders the energy of photoinduced charge carriers. To solve this problem, rational design of a dual-function reaction system, in which photocatalytic oxidation and reduction reactions operate in a harmonious manner, will be an effective way.

AUTHOR INFORMATION

Corresponding Authors

Kang-Qiang Lu − *College of Materials, Metallurgical and Chemistry, Jiangxi University of Science and Technology, Ganzhou 341000, P. R. China; College of Chemistry, State Key Laboratory of Photocatalysis on Energy and Environment, Fuzhou University, Fuzhou 350116, P. R. China*; Email: kqlu@jxust.edu.cn

Yi-Jun Xu − *College of Chemistry, State Key Laboratory of Photocatalysis on Energy and Environment, Fuzhou University, Fuzhou 350116, P. R. China*; orcid.org/0000-0002-2195-1695; Email: yjxu@fzu.edu.cn

Authors

Yue-Hua Li − *College of Chemistry, State Key Laboratory of Photocatalysis on Energy and Environment, Fuzhou University, Fuzhou 350116, P. R. China*

Zi-Rong Tang − *College of Chemistry, State Key Laboratory of Photocatalysis on Energy and Environment, Fuzhou University, Fuzhou 350116, P. R. China*; orcid.org/0000-0002-6564-3539

Complete contact information is available at: https://pubs.acs.org/10.1021/acsmaterialsau.1c00022

Notes

The authors declare no competing financial interest.

ACKNOWLEDGMENTS

The support from the National Natural Science Foundation of China (NSFC) (22072023, 21872029, U1463204, 21173045), the Program for National Science and Technology Innovation Leading Talents (00387072), the Natural Science Foundation (NSF) of Fujian Province for Distinguished Young Investigator Rolling Grant (2017J07002), NSF of Fujian Province (2019J0106), the Program for Leading Talents of Fujian Universities, the first Program of Fujian Province for Top Creative Young Talents, the China Postdoctoral Science Foundation (2021M692456), and the Young Science Foundation of Jiangxi Province Education Office (GJJ200846).

REFERENCES

(1) Zhang, N.; Yang, M.-Q.; Liu, S.; Sun, Y.; Xu, Y.-J. Waltzing with the Versatile Platform of Graphene to Synthesize Composite Photocatalysts. *Chem. Rev.* **2015**, *115*, 10307−10377.

(2) Wang, B.; Gu, D.; Ji, L.; Wu, H. Photocatalysis: A Novel Approach to Efficient Demulsification. *Catal. Commun.* **2016**, *75*, 83−86.

(3) Yang, M.-Q.; Zhang, N.; Pagliaro, M.; Xu, Y.-J. Artificial Photosynthesis over Graphene-Semiconductor Composites. Are We Getting Better? *Chem. Soc. Rev.* **2014**, *43*, 8240−8254.

(4) Li, A.; Zhu, W.; Li, C.; Wang, T.; Gong, J. Rational Design of Yolk−Shell Nanostructures for Photocatalysis. *Chem. Soc. Rev.* **2019**, *48*, 1874−1907.

(5) Cannalire, R.; Pelliccia, S.; Sancineto, L.; Novellino, E.; Tron, G. C.; Giustiniano, M. Visible Light Photocatalysis in the Late-Stage Functionalization of Pharmaceutically Relevant Compounds. *Chem. Soc. Rev.* **2021**, *50*, 766−897.

(6) Zhong, S.; Xi, Y.; Wu, S.; Liu, Q.; Zhao, L.; Bai, S. Hybrid Cocatalysts in Semiconductor-Based Photocatalysis and Photoelectrocatalysis. *J. Mater. Chem. A* **2020**, *8*, 14863−14894.

(7) Yadav, D.; Kumar, A.; Kim, J. Y.; Park, N.-J.; Baeg, J.-O. Interfacially Synthesized 2D COF Thin Film Photocatalyst: Efficient Photocatalyst for Solar Formic Acid Production from CO_2 and Fine Chemical Synthesis. *J. Mater. Chem. A* **2021**, *9*, 9573−9580.

(8) Chen, R.; Wang, Y.; Ma, Y.; Mal, A.; Gao, X.-Y.; Gao, L.; Qiao, L.; Li, X.-B.; Wu, L.-Z.; Wang, C. Rational Design of Isostructural 2D Porphyrin-Based Covalent Organic Frameworks for Tunable Photocatalytic Hydrogen Evolution. *Nat. Commun.* **2021**, *12*, 1354.

(9) Nakada, A.; Kato, D.; Nelson, R.; Takahira, H.; Yabuuchi, M.; Higashi, M.; Suzuki, H.; Kirsanova, M.; Kakudou, N.; Tassel, C.; Yamamoto, T.; Brown, C. M.; Dronskowski, R.; Saeki, A.; Abakumov, A.; Kageyama, H.; Abe, R. Conduction Band Control of Oxyhalides with a Triple-Fluorite Layer for Visible Light Photocatalysis. *J. Am. Chem. Soc.* **2021**, *143*, 2491−2499.

(10) Michelin, C.; Hoffmann, N. Photosensitization and Photocatalysis-Perspectives in Organic Synthesis. *ACS Catal.* **2018**, *8*, 12046−12055.

(11) Chen, L.; Tang, J.; Song, L.-N.; Chen, P.; He, J.; Au, C.-T.; Yin, S.-F. Heterogeneous Photocatalysis for Selective Oxidation of Alcohols and Hydrocarbons. *Appl. Catal., B* **2019**, *242*, 379−388.

(12) Betancourt, A. P.; Goswami, D. Y.; Bhethanabotla, V. R.; Kuhn, J. N. Scalable and Stable Silica-Coated Silver Nanoparticles, Produced by Electron Beam Evaporation and Rapid Thermal Annealing, for Plasmon-Enhanced Photocatalysis. *Catal. Commun.* **2021**, *149*, 106213.

(13) Cravotto, G.; Borretto, E.; Oliverio, M.; Procopio, A.; Penoni, A. Organic Reactions in Water or Biphasic Aqueous Systems under Sonochemical Conditions. A Review on Catalytic Effects. *Catal. Commun.* **2015**, *63*, 2−9.

(14) Li, X.; Wang, W.; Dong, F.; Zhang, Z.; Han, L.; Luo, X.; Huang, J.; Feng, Z.; Chen, Z.; Jia, G.; Zhang, T. Recent Advances in Noncontact External-Field-Assisted Photocatalysis: From Fundamentals to Applications. *ACS Catal.* **2021**, *11*, 4739−4769.

(15) Baek, M.-H.; Hong, J.-S.; Yoon, J.-W.; Suh, J.-K. Photocatalytic Degradation of Humic Acid by Fe-TiO_2 Supported on Spherical Activated Carbon with Enhanced Activity. *Int. J. Photoenergy* **2013**, *2013*, 296821.
(16) Wang, N.; Zhai, Y.; Yang, Y.; Yang, X.; Zhu, Z. Electrostatic Assembly of Superwetting Porous Nanofibrous Membrane Toward Oil-In-Water Microemulsion Separation. *Chem. Eng. J.* **2018**, *354*, 463−472.
(17) Rej, S.; Bisetto, M.; Naldoni, A.; Fornasiero, P. Well-Defined Cu_2O Photocatalysts for Solar Fuels and Chemicals. *J. Mater. Chem. A* **2021**, *9*, 5915−5951.
(18) Kröger, J.; Jiménez-Solano, A.; Savasci, G.; Rovó, P.; Moudrakovski, I.; Küster, K.; Schlomberg, H.; Vignolo-González, H. A.; Duppel, V.; Grunenberg, L.; Dayan, C. B.; Sitti, M.; Podjaski, F.; Ochsenfeld, C.; Lotsch, B. V. Interfacial Engineering for Improved Photocatalysis in a Charge Storing 2D Carbon Nitride: Melamine Functionalized Poly(heptazine imide). *Adv. Energy Mater.* **2021**, *11*, 2003016.
(19) Zhang, L.; Ran, J.; Qiao, S.-Z.; Jaroniec, M. Characterization of Semiconductor Photocatalysts. *Chem. Soc. Rev.* **2019**, *48*, 5184−5206.
(20) Wang, Z.; Huang, J.; Mao, J.; Guo, Q.; Chen, Z.; Lai, Y. Metal−Organic Frameworks and Their Derivatives with Graphene Composites: Preparation and Applications in Electrocatalysis and Photocatalysis. *J. Mater. Chem. A* **2020**, *8*, 2934−2961.
(21) Qiu, B.; Xing, M.; Zhang, J. Mesoporous TiO_2 Nanocrystals Grown in Situ on Graphene Aerogels for High Photocatalysis and Lithium-Ion Batteries. *J. Am. Chem. Soc.* **2014**, *136*, 5852−5855.
(22) Kisch, H. Semiconductor Photocatalysis for Chemoselective Radical Coupling Reactions. *Acc. Chem. Res.* **2017**, *50*, 1002−1010.
(23) Giannakoudakis, D. A.; Qayyum, A.; Łomot, D.; Besenhard, M. O.; Lisovytskiy, D.; Bandosz, T. J.; Colmenares, J. C. Boosting the Photoactivity of Grafted Titania: Ultrasound-Driven Synthesis of a Multi-Phase Heterogeneous Nano-Architected Photocatalyst. *Adv. Funct. Mater.* **2021**, *31*, 2007115.
(24) Yuan, Z.; Xiao, X.; Li, J.; Zhao, Z.; Yu, D.; Li, Q. Self-Assembled Graphene-Based Architectures and Their Applications. *Adv. Sci.* **2018**, *5*, 1700626.
(25) Liu, G.; Zhen, C.; Kang, Y.; Wang, L.; Cheng, H.-M. Unique Physicochemical Properties of Two-Dimensional Light Absorbers Facilitating Photocatalysis. *Chem. Soc. Rev.* **2018**, *47*, 6410−6444.
(26) Nosaka, Y.; Nosaka, A. Y. Generation and Detection of Reactive Oxygen Species in Photocatalysis. *Chem. Rev.* **2017**, *117*, 11302−11336.
(27) Zhao, F.; Feng, Y.; Wang, Y.; Zhang, X.; Liang, X.; Li, Z.; Zhang, F.; Wang, T.; Gong, J.; Feng, W. Two-Dimensional Gersiloxenes with Tunable Bandgap for Photocatalytic H_2 Evolution and CO_2 Photoreduction to CO. *Nat. Commun.* **2020**, *11*, 1443.
(28) Huang, H.; Shi, H.; Das, P.; Qin, J.; Li, Y.; Wang, X.; Su, F.; Wen, P.; Li, S.; Lu, P.; Liu, F.; Li, Y.; Zhang, Y.; Wang, Y.; Wu, Z.-S.; Cheng, H.-M. The Chemistry and Promising Applications of Graphene and Porous Graphene Materials. *Adv. Funct. Mater.* **2020**, *30*, 1909035.
(29) Vicarelli, L.; Heerema, S. J.; Dekker, C.; Zandbergen, H. W. Controlling Defects in Graphene for Optimizing the Electrical Properties of Graphene Nanodevices. *ACS Nano* **2015**, *9*, 3428−3435.
(30) Pan, S.; Aksay, I. A. Factors Controlling the Size of Graphene Oxide Sheets Produced via the Graphite Oxide Route. *ACS Nano* **2011**, *5*, 4073−4083.
(31) Luo, J.; Cote, L. J.; Tung, V. C.; Tan, A. T. L.; Goins, P. E.; Wu, J.; Huang, J. Graphene Oxide Nanocolloids. *J. Am. Chem. Soc.* **2010**, *132*, 17667−17669.
(32) Luo, J.; Yang, L.; Sun, D.; Gao, Z.; Jiao, K.; Zhang, J. Graphene Oxide "Surfactant"-Directed Tunable Concentration of Graphene Dispersion. *Small* **2020**, *16*, 2003426.
(33) Kim, J.; Cote, L. J.; Kim, F.; Yuan, W.; Shull, K. R.; Huang, J. Graphene Oxide Sheets at Interfaces. *J. Am. Chem. Soc.* **2010**, *132*, 8180−8186.
(34) Xia, Y.; Tian, Z.; Heil, T.; Meng, A.; Cheng, B.; Cao, S.; Yu, J.; Antonietti, M. Highly Selective CO_2 Capture and Its Direct Photochemical Conversion on Ordered 2D/1D Heterojunctions. *Joule* **2019**, *3*, 2792−2805.
(35) Dong, Y.; Li, J.; Shi, L.; Xu, J.; Wang, X.; Guo, Z.; Liu, W. Graphene Oxide−Iron Complex: Synthesis, Characterization and Visible-Light-Driven Photocatalysis. *J. Mater. Chem. A* **2013**, *1*, 644−650.
(36) Bera, R.; Kundu, S.; Patra, A. 2D Hybrid Nanostructure of Reduced Graphene Oxide−CdS Nanosheet for Enhanced Photocatalysis. *ACS Appl. Mater. Interfaces* **2015**, *7*, 13251−13259.
(37) Xin, X.; Li, S.-H.; Zhang, N.; Tang, Z.-R.; Xu, Y.-J. 3D Graphene/AgBr/Ag Cascade Aerogel for Efficient Photocatalytic Disinfection. *Appl. Catal., B* **2019**, *245*, 343−350.
(38) Ding, Z.; Liang, J.; Zhang, W.; Wang, W.; Geng, R.; Wang, Y.; Li, P.; Fan, Q. Efficiency and Active Sites of the Synergetic Sorption and Photocatalysis in Cr(VI) Decontamination on a 3D Oxidized Graphene Ribbon Framework. *J. Mater. Chem. A* **2020**, *8*, 11362−11369.
(39) Lu, K.-Q.; Xin, X.; Zhang, N.; Tang, Z.-R.; Xu, Y.-J. Photoredox Catalysis over Graphene Aerogel-Supported Composites. *J. Mater. Chem. A* **2018**, *6*, 4590−4604.
(40) Yeh, T.-F.; Cihlář, J.; Chang, C.-Y.; Cheng, C.; Teng, H. Roles of Graphene Oxide in Photocatalytic Water Splitting. *Mater. Today* **2013**, *16*, 78−84.
(41) Zhang, L.; Zhang, Q.; Xie, H.; Guo, J.; Lyu, H.; Li, Y.; Sun, Z.; Wang, H.; Guo, Z. Electrospun Titania Nanofibers Segregated by Graphene Oxide for Improved Visible Light Photocatalysis. *Appl. Catal., B* **2017**, *201*, 470−478.
(42) Eigler, S.; Hirsch, A. Chemistry with Graphene and Graphene Oxide—Challenges for Synthetic Chemists. *Angew. Chem., Int. Ed.* **2014**, *53*, 7720−7738.
(43) Low, J.; Yu, J.; Ho, W. Graphene-Based Photocatalysts for CO_2 Reduction to Solar Fuel. *J. Phys. Chem. Lett.* **2015**, *6*, 4244−4251.
(44) Quan, Q.; Lin, X.; Zhang, N.; Xu, Y. Graphene and Its Derivatives as Versatile Templates for Materials Synthesis and Functional Applications. *Nanoscale* **2017**, *9*, 2398−2416.
(45) Zhang, N.; Zhang, Y.; Xu, Y.-J. Recent Progress on Graphene-Based Photocatalysts: Current Status and Future Perspectives. *Nanoscale* **2012**, *4*, 5792−5813.
(46) Chabot, V.; Higgins, D.; Yu, A.; Xiao, X.; Chen, Z.; Zhang, J. A Review of Graphene and Graphene Oxide Sponge: Material Synthesis and Applications to Energy and the Environment. *Energy Environ. Sci.* **2014**, *7*, 1564−1596.
(47) Bie, C.; Yu, H.; Cheng, B.; Ho, W.; Fan, J.; Yu, J. Design, Fabrication, and Mechanism of Nitrogen-Doped Graphene-Based Photocatalyst. *Adv. Mater.* **2021**, *33*, 2003521.
(48) Dreyer, D. R.; Park, S.; Bielawski, C. W.; Ruoff, R. S. The Chemistry of Graphene Oxide. *Chem. Soc. Rev.* **2010**, *39*, 228−240.
(49) Liu, B.; Xie, J.; Ma, H.; Zhang, X.; Pan, Y.; Lv, J.; Ge, H.; Ren, N.; Su, H.; Xie, X.; Huang, L.; Huang, W. From Graphite to Graphene Oxide and Graphene Oxide Quantum Dots. *Small* **2017**, *13*, 1601001.
(50) Chua, C. K.; Pumera, M. Graphene Oxide: Light and Atmosphere Affect the Quasi-equilibrium States of Graphite Oxide and Graphene Oxide Powders. *Small* **2015**, *11*, 1265−1265.
(51) Prekodravac, J. R.; Kepić, D. P.; Colmenares, J. C.; Giannakoudakis, D. A.; Jovanović, S. P. A Comprehensive Review on Selected Graphene Synthesis Methods: From Electrochemical Exfoliation through Rapid Thermal Annealing Towards Biomass Pyrolysis. *J. Mater. Chem. C* **2021**, *9*, 6722−6748.
(52) Brodie, B. C. XIII. On the Atomic Weight of Graphite. *Philos. Trans. R. Soc. London* **1859**, *149*, 249−259.
(53) Stankovich, S.; Dikin, D. A.; Piner, R. D.; Kohlhaas, K. A.; Kleinhammes, A.; Jia, Y.; Wu, Y.; Nguyen, S. T.; Ruoff, R. S. Synthesis of Graphene-Based Nanosheets via Chemical Reduction of Exfoliated Graphite Oxide. *Carbon* **2007**, *45*, 1558−1565.
(54) Stankovich, S.; Dikin, D. A.; Dommett, G. H. B.; Kohlhaas, K. M.; Zimney, E. J.; Stach, E. A.; Piner, R. D.; Nguyen, S. T.; Ruoff, R. S. Graphene-Based Composite Materials. *Nature* **2006**, *442*, 282−286.
(55) Dikin, D. A.; Stankovich, S.; Zimney, E. J.; Piner, R. D.; Dommett, G. H. B.; Evmenenko, G.; Nguyen, S. T.; Ruoff, R. S.

Preparation and Characterization of Graphene Oxide Paper. *Nature* **2007**, *448*, 457−460.
(56) Marcano, D. C.; Kosynkin, D. V.; Berlin, J. M.; Sinitskii, A.; Sun, Z.; Slesarev, A.; Alemany, L. B.; Lu, W.; Tour, J. M. Improved Synthesis of Graphene Oxide. *ACS Nano* **2010**, *4*, 4806−4814.
(57) Hummers, W. S.; Offeman, R. E. Preparation of Graphitic Oxide. *J. Am. Chem. Soc.* **1958**, *80*, 1339−1339.
(58) Kang, J. H.; Kim, T.; Choi, J.; Park, J.; Kim, Y. S.; Chang, M. S.; Jung, H.; Park, K. T.; Yang, S. J.; Park, C. R. Hidden Second Oxidation Step of Hummers Method. *Chem. Mater.* **2016**, *28*, 756−764.
(59) Zhao, J.; Pei, S.; Ren, W.; Gao, L.; Cheng, H.-M. Efficient Preparation of Large-Area Graphene Oxide Sheets for Transparent Conductive Films. *ACS Nano* **2010**, *4*, 5245−5252.
(60) Sun, T.; Fabris, S. Mechanisms for Oxidative Unzipping and Cutting of Graphene. *Nano Lett.* **2012**, *12*, 17−21.
(61) Li, X.; Yu, J.; Wageh, S.; Al-Ghamdi, A. A.; Xie, J. Graphene in Photocatalysis: A Review. *Small* **2016**, *12*, 6640−6696.
(62) Peng, L.; Xu, Z.; Liu, Z.; Wei, Y.; Sun, H.; Li, Z.; Zhao, X.; Gao, C. An Iron-Based Green Approach to 1-h Production of Single-Layer Graphene Oxide. *Nat. Commun.* **2015**, *6*, 5716.
(63) Chen, D.; Lin, Z.; Sartin, M. M.; Huang, T.-X.; Liu, J.; Zhang, Q.; Han, L.; Li, J.-F.; Tian, Z.-Q.; Zhan, D. Photosynergetic Electrochemical Synthesis of Graphene Oxide. *J. Am. Chem. Soc.* **2020**, *142*, 6516−6520.
(64) Pedram, M. Z.; Kazemeini, M.; Fattahi, M.; Amjadian, A. A Physicochemical Evaluation of Modified HZSM-5 Catalyst Utilized for Production of Dimethyl Ether From Methanol. *Pet. Sci. Technol.* **2014**, *32*, 904−911.
(65) Padmajan Sasikala, S.; Lim, J.; Kim, I. H.; Jung, H. J.; Yun, T.; Han, T. H.; Kim, S. O. Graphene Oxide Liquid Crystals: A Frontier 2D Soft Material for Graphene-Based Functional Materials. *Chem. Soc. Rev.* **2018**, *47*, 6013−6045.
(66) Feng, H.; Cheng, R.; Zhao, X.; Duan, X.; Li, J. A Low-Temperature Method to Produce Highly Reduced Graphene Oxide. *Nat. Commun.* **2013**, *4*, 1539.
(67) Li, M.; Wang, Y.; Tang, P.; Xie, N.; Zhao, Y.; Liu, X.; Hu, G.; Xie, J.; Zhao, Y.; Tang, J.; Zhang, T.; Ma, D. Graphene with Atomic-Level In-Plane Decoration of h-BN Domains for Efficient Photocatalysis. *Chem. Mater.* **2017**, *29*, 2769−2776.
(68) Staudenmaier, L. Verfahren Zur Darstellung Der Graphitsäure. *Ber. Dtsch. Chem. Ges.* **1898**, *31*, 1481−1487.
(69) Hofmann, U.; König, E. Untersuchungen über Graphitoxyd. *Z. Anorg. Allg. Chem.* **1937**, *234*, 311−336.
(70) Kovtyukhova, N. I.; Ollivier, P. J.; Martin, B. R.; Mallouk, T. E.; Chizhik, S. A.; Buzaneva, E. V.; Gorchinskiy, A. D. Layer-by-Layer Assembly of Ultrathin Composite Films from Micron-Sized Graphite Oxide Sheets and Polycations. *Chem. Mater.* **1999**, *11*, 771−778.
(71) Hirata, M.; Gotou, T.; Horiuchi, S.; Fujiwara, M.; Ohba, M. Thin-Film Particles of Graphite Oxide: High-Yield Synthesis and Flexibility of the Particles. *Carbon* **2004**, *42*, 2929−2937.
(72) Ang, P. K.; Wang, S.; Bao, Q.; Thong, J. T. L.; Loh, K. P. High-Throughput Synthesis of Graphene by Intercalation−Exfoliation of Graphite Oxide and Study of Ionic Screening in Graphene Transistor. *ACS Nano* **2009**, *3*, 3587−3594.
(73) Marcano, D. C.; Kosynkin, D. V.; Berlin, J. M.; Sinitskii, A.; Sun, Z.; Slesarev, A. S.; Alemany, L. B.; Lu, W.; Tour, J. M. Correction to Improved Synthesis of Graphene Oxide. *ACS Nano* **2018**, *12*, 2078−2078.
(74) Eigler, S.; Enzelberger-Heim, M.; Grimm, S.; Hofmann, P.; Kroener, W.; Geworski, A.; Dotzer, C.; Röckert, M.; Xiao, J.; Papp, C.; Lytken, O.; Steinrück, H.-P.; Müller, P.; Hirsch, A. Wet Chemical Synthesis of Graphene. *Adv. Mater.* **2013**, *25*, 3583−3587.
(75) Dimiev, A. M.; Tour, J. M. Mechanism of Graphene Oxide Formation. *ACS Nano* **2014**, *8*, 3060−3068.
(76) Agegnehu, A. K.; Pan, C.-J.; Rick, J.; Lee, J.-F.; Su, W.-N.; Hwang, B.-J. Enhanced Hydrogen Generation by Cocatalytic Ni and NiO Nanoparticles Loaded on Graphene Oxide Sheets. *J. Mater. Chem.* **2012**, *22*, 13849−13854.
(77) De Silva, K. K. H.; Huang, H. H.; Joshi, R. K.; Yoshimura, M. Chemical Reduction of Graphene Oxide Using Green Reductants. *Carbon* **2017**, *119*, 190−199.
(78) Chua, C. K.; Pumera, M. Chemical Reduction of Graphene Oxide: A Synthetic Chemistry Viewpoint. *Chem. Soc. Rev.* **2014**, *43*, 291−312.
(79) Gao, W.; Alemany, L. B.; Ci, L.; Ajayan, P. M. New Insights into the Structure and Reduction of Graphite Oxide. *Nat. Chem.* **2009**, *1*, 403−408.
(80) Lang, X.; Chen, X.; Zhao, J. Heterogeneous Visible Light Photocatalysis for Selective Organic Transformations. *Chem. Soc. Rev.* **2014**, *43*, 473−486.
(81) He, H.; Klinowski, J.; Forster, M.; Lerf, A. A New Structural Model for Graphite Oxide. *Chem. Phys. Lett.* **1998**, *287*, 53−56.
(82) Xiang, Q.; Cheng, B.; Yu, J. Graphene-Based Photocatalysts for Solar-Fuel Generation. *Angew. Chem., Int. Ed.* **2015**, *54*, 11350−11366.
(83) Han, C.; Zhang, N.; Xu, Y.-J. Structural Diversity of Graphene Materials and Their Multifarious Roles in Heterogeneous Photocatalysis. *Nano Today* **2016**, *11*, 351−372.
(84) Erickson, K.; Erni, R.; Lee, Z.; Alem, N.; Gannett, W.; Zettl, A. Determination of the Local Chemical Structure of Graphene Oxide and Reduced Graphene Oxide. *Adv. Mater.* **2010**, *22*, 4467−4472.
(85) Zhu, Y.; Murali, S.; Cai, W.; Li, X.; Suk, J. W.; Potts, J. R.; Ruoff, R. S. Graphene and Graphene Oxide: Synthesis, Properties, and Applications. *Adv. Mater.* **2010**, *22*, 3906−3924.
(86) Yu, S.-H.; Conte, D. E.; Baek, S.; Lee, D.-C.; Park, S.-K.; Lee, K. J.; Piao, Y.; Sung, Y.-E.; Pinna, N. Structure-Properties Relationship in Iron Oxide-Reduced Graphene Oxide Nanostructures for Li-Ion Batteries. *Adv. Funct. Mater.* **2013**, *23*, 4293−4305.
(87) Yang, M.-Q.; Han, C.; Zhang, N.; Xu, Y.-J. Precursor Chemistry Matters in Boosting Photoredox Activity of Graphene/Semiconductor Composites. *Nanoscale* **2015**, *7*, 18062−18070.
(88) Chua, C. K.; Pumera, M. Reduction of Graphene Oxide with Substituted Borohydrides. *J. Mater. Chem. A* **2013**, *1*, 1892−1898.
(89) Wei, Z.; Wang, D.; Kim, S.; Kim, S.-Y.; Hu, Y.; Yakes, M. K.; Laracuente, A. R.; Dai, Z.; Marder, S. R.; Berger, C.; King, W. P.; de Heer, W. A.; Sheehan, P. E.; Riedo, E. Nanoscale Tunable Reduction of Graphene Oxide for Graphene Electronics. *Science* **2010**, *328*, 1373−1376.
(90) Liu, Q.; Zhang, M.; Huang, L.; Li, Y.; Chen, J.; Li, C.; Shi, G. High-Quality Graphene Ribbons Prepared from Graphene Oxide Hydrogels and Their Application for Strain Sensors. *ACS Nano* **2015**, *9*, 12320−12326.
(91) Moon, I. K.; Lee, J.; Ruoff, R. S.; Lee, H. Reduced Graphene Oxide by Chemical Graphitization. *Nat. Commun.* **2010**, *1*, 73.
(92) Li, Z.; Zhang, W.; Luo, Y.; Yang, J.; Hou, J. G. How Graphene Is Cut upon Oxidation? *J. Am. Chem. Soc.* **2009**, *131*, 6320−6321.
(93) Upadhyay, R. K.; Soin, N.; Roy, S. S. Role of Graphene/Metal Oxide Composites as Photocatalysts, Adsorbents and Disinfectants in Water Treatment: A Review. *RSC Adv.* **2014**, *4*, 3823−3851.
(94) Georgakilas, V.; Tiwari, J. N.; Kemp, K. C.; Perman, J. A.; Bourlinos, A. B.; Kim, K. S.; Zboril, R. Noncovalent Functionalization of Graphene and Graphene Oxide for Energy Materials, Biosensing, Catalytic, and Biomedical Applications. *Chem. Rev.* **2016**, *116*, 5464−5519.
(95) Lu, K.-Q.; Li, Y.-H.; Zhang, F.; Qi, M.-Y.; Chen, X.; Tang, Z.-R.; Yamada, Y. M. A.; Anpo, M.; Conte, M.; Xu, Y.-J. Rationally Designed Transition Metal Hydroxide Nanosheet Arrays on Graphene for Artificial CO_2 Reduction. *Nat. Commun.* **2020**, *11*, 5181.
(96) Gao, X.; Zhang, J.; Ju, P.; Liu, J.; Ji, L.; Liu, X.; Ma, T.; Chen, L.; Li, H.; Zhou, H.; Chen, J. Shear-Induced Interfacial Structural Conversion of Graphene Oxide to Graphene at Macroscale. *Adv. Funct. Mater.* **2020**, *30*, 2004498.
(97) Jalili, R.; Aboutalebi, S. H.; Esrafilzadeh, D.; Konstantinov, K.; Moulton, S. E.; Razal, J. M.; Wallace, G. G. Organic Solvent-Based Graphene Oxide Liquid Crystals: A Facile Route toward the Next

Generation of Self-Assembled Layer-by-Layer Multifunctional 3D Architectures. *ACS Nano* **2013**, *7*, 3981−3990.
(98) Paredes, J. I.; Villar-Rodil, S.; Martínez-Alonso, A.; Tascón, J. M. D. Graphene Oxide Dispersions in Organic Solvents. *Langmuir* **2008**, *24*, 10560−10564.
(99) Kim, F.; Cote, L. J.; Huang, J. Graphene Oxide: Surface Activity and Two-Dimensional Assembly. *Adv. Mater.* **2010**, *22*, 1954−1958.
(100) Shundo, A.; Hori, K.; Penaloza, D. P.; Matsumoto, Y.; Okumura, Y.; Kikuchi, H.; Lee, K. E.; Kim, S. O.; Tanaka, K. Hierarchical Spatial Heterogeneity in Liquid Crystals Composed of Graphene Oxides. *Phys. Chem. Chem. Phys.* **2016**, *18*, 22399−22406.
(101) Bansal, P.; Panwar, A. S.; Bahadur, D. Molecular-Level Insights into the Stability of Aqueous Graphene Oxide Dispersions. *J. Phys. Chem. C* **2017**, *121*, 9847−9859.
(102) Lu, K.-Q.; Yuan, L.; Xin, X.; Xu, Y.-J. Hybridization of Graphene Oxide with Commercial Graphene for Constructing 3D Metal-Free Aerogel with Enhanced Photocatalysis. *Appl. Catal., B* **2018**, *226*, 16−22.
(103) Shih, C.-J.; Lin, S.; Sharma, R.; Strano, M. S.; Blankschtein, D. Understanding the pH-Dependent Behavior of Graphene Oxide Aqueous Solutions: A Comparative Experimental and Molecular Dynamics Simulation Study. *Langmuir* **2012**, *28*, 235−241.
(104) Trapalis, A.; Todorova, N.; Giannakopoulou, T.; Boukos, N.; Speliotis, T.; Dimotikali, D.; Yu, J. TiO_2/Graphene Composite Photocatalysts for NOx Removal: A Comparison of Surfactant-Stabilized Graphene and Reduced Graphene Oxide. *Appl. Catal., B* **2016**, *180*, 637−647.
(105) Gudarzi, M. M. Colloidal Stability of Graphene Oxide: Aggregation in Two Dimensions. *Langmuir* **2016**, *32*, 5058−5068.
(106) Tang, H.; Liu, D.; Zhao, Y.; Yang, X.; Lu, J.; Cui, F. Molecular Dynamics Study of the Aggregation Process of Graphene Oxide in Water. *J. Phys. Chem. C* **2015**, *119*, 26712−26718.
(107) Jin, Y.; Xu, Z.; Guo, Y.; Yang, X. Molecular-Level Recognition of Interaction Mechanism between Graphene Oxides in Solvent Media. *J. Phys. Chem. C* **2018**, *122*, 4063−4072.
(108) Berger, C.; Song, Z.; Li, X.; Wu, X.; Brown, N.; Naud, C.; Mayou, D.; Li, T.; Hass, J.; Marchenkov, A. N.; Conrad, E. H.; First, P. N.; de Heer, W. A. Electronic Confinement and Coherence in Patterned Epitaxial Graphene. *Science* **2006**, *312*, 1191−1196.
(109) Ito, J.; Nakamura, J.; Natori, A. Semiconducting Nature of the Oxygen-Adsorbed Graphene Sheet. *J. Appl. Phys.* **2008**, *103*, 113712.
(110) Burghard, M.; Klauk, H.; Kern, K. Carbon-Based Field-Effect Transistors for Nanoelectronics. *Adv. Mater.* **2009**, *21*, 2586−2600.
(111) Liu, H.; Ryu, S.; Chen, Z.; Steigerwald, M. L.; Nuckolls, C.; Brus, L. E. Photochemical Reactivity of Graphene. *J. Am. Chem. Soc.* **2009**, *131*, 17099−17101.
(112) Xiang, Q.; Yu, J.; Jaroniec, M. Graphene-Based Semiconductor Photocatalysts. *Chem. Soc. Rev.* **2012**, *41*, 782−796.
(113) Yeh, T.-F.; Chan, F.-F.; Hsieh, C.-T.; Teng, H. Graphite Oxide with Different Oxygenated Levels for Hydrogen and Oxygen Production from Water Under Illumination: The Band Positions of Graphite Oxide. *J. Phys. Chem. C* **2011**, *115*, 22587−22597.
(114) Yeh, T.-F.; Syu, J.-M.; Cheng, C.; Chang, T.-H.; Teng, H. Graphite Oxide as a Photocatalyst for Hydrogen Production from Water. *Adv. Funct. Mater.* **2010**, *20*, 2255−2262.
(115) Bagri, A.; Mattevi, C.; Acik, M.; Chabal, Y. J.; Chhowalla, M.; Shenoy, V. B. Structural Evolution During the Reduction of Chemically Derived Graphene Oxide. *Nat. Chem.* **2010**, *2*, 581−587.
(116) Yeh, T.-F.; Chen, S.-J.; Teng, H. Synergistic Effect of Oxygen and Nitrogen Functionalities for Graphene-Based Quantum Dots Used in Photocatalytic H_2 Production from Water Decomposition. *Nano Energy* **2015**, *12*, 476−485.
(117) Yeh, T.-F.; Teng, C.-Y.; Chen, S.-J.; Teng, H. Nitrogen-Doped Graphene Oxide Quantum Dots as Photocatalysts for Overall Water-Splitting under Visible Light Illumination. *Adv. Mater.* **2014**, *26*, 3297−3303.
(118) Zhang, N.; Xu, Y. The Endeavour to Advance Graphene−Semiconductor Composite-Based Photocatalysis. *CrystEngComm* **2016**, *18*, 24−37.
(119) Zhang, Y.; Tang, Z.-R.; Fu, X.; Xu, Y.-J. Engineering the Unique 2D Mat of Graphene to Achieve Graphene-TiO_2 Nanocomposite for Photocatalytic Selective Transformation: What Advantage does Graphene Have over Its Forebear Carbon Nanotube? *ACS Nano* **2011**, *5*, 7426−7435.
(120) Giannakoudakis, D. A.; Vikrant, K.; LaGrow, A. P.; Lisovytskiy, D.; Kim, K.-H.; Bandosz, T. J.; Carlos Colmenares, J. Scrolled Titanate Nanosheet Composites with Reduced Graphite Oxide for Photocatalytic and Adsorptive Removal of Toxic Vapors. *Chem. Eng. J.* **2021**, *415*, 128907.
(121) Garmroudi, A.; Kheirollahi, M.; Mousavi, S. A.; Fattahi, M.; Mahvelati, E. H. Effects of Graphene Oxide/TiO_2 Nanocomposite, Graphene Oxide Nanosheets and Cedr Extraction Solution on IFT Reduction and Ultimate Oil Recovery from a Carbonate Rock. *Petroleum* **2020**, DOI: 10.1016/j.petlm.2020.10.002.
(122) Posudievsky, O. Y.; Kozarenko, O. A.; Khazieieva, O. A.; Koshechko, V. G.; Pokhodenko, V. D. Ultrasound-Free Preparation of Graphene Oxide from Mechanochemically Oxidized Graphite. *J. Mater. Chem. A* **2013**, *1*, 6658−6663.
(123) Zhang, Y.; Tang, Z.-R.; Fu, X.; Xu, Y.-J. TiO_2−Graphene Nanocomposites for Gas-Phase Photocatalytic Degradation of Volatile Aromatic Pollutant: Is TiO_2−Graphene Truly Different from Other TiO_2−Carbon Composite Materials? *ACS Nano* **2010**, *4*, 7303−7314.
(124) Lu, K.-Q.; Chen, Y.; Xin, X.; Xu, Y.-J. Rational Utilization of Highly Conductive, Commercial Elicarb Graphene to Advance the Graphene-Semiconductor Composite Photocatalysis. *Appl. Catal., B* **2018**, *224*, 424−432.
(125) Wang, H.-X.; Wang, Q.; Zhou, K.-G.; Zhang, H.-L. Graphene in Light: Design, Synthesis and Applications of Photo-active Graphene and Graphene-Like Materials. *Small* **2013**, *9*, 1266−1283.
(126) Paton, K. R.; Varrla, E.; Backes, C.; Smith, R. J.; Khan, U.; O'Neill, A.; Boland, C.; Lotya, M.; Istrate, O. M.; King, P.; Higgins, T.; Barwich, S.; May, P.; Puczkarski, P.; Ahmed, I.; Moebius, M.; Pettersson, H.; Long, E.; Coelho, J.; O'Brien, S. E.; McGuire, E. K.; Sanchez, B. M.; Duesberg, G. S.; McEvoy, N.; Pennycook, T. J.; Downing, C.; Crossley, A.; Nicolosi, V.; Coleman, J. N. Scalable Production of Large Quantities of Defect-Free Few-Layer Graphene by Shear Exfoliation in Liquids. *Nat. Mater.* **2014**, *13*, 624−630.
(127) Liang, Y. T.; Vijayan, B. K.; Gray, K. A.; Hersam, M. C. Minimizing Graphene Defects Enhances Titania Nanocomposite-Based Photocatalytic Reduction of CO_2 for Improved Solar Fuel Production. *Nano Lett.* **2011**, *11*, 2865−2870.
(128) Cheng, X.; Liu, H.; Chen, Q.; Li, J.; Wang, P. Preparation of Graphene Film Decorated TiO_2 Nano-Tube Array Photoelectrode and Its Enhanced Visible Light Photocatalytic Mechanism. *Carbon* **2014**, *66*, 450−458.
(129) Joshi, B.; Yoon, H.; Na, S. H.; Choi, J. Y.; Yoon, S. G. Enhanced Photocatalytic Performance of Graphene−ZnO Nanoplatelet Composite Thin Films Prepared by Electrostatic Spray Deposition. *Ceram. Int.* **2014**, *40*, 3647−3654.
(130) Akhavan, O.; Ghaderi, E. Photocatalytic Reduction of Graphene Oxide Nanosheets on TiO_2 Thin Film for Photoinactivation of Bacteria in Solar Light Irradiation. *J. Phys. Chem. C* **2009**, *113*, 20214−20220.
(131) Tang, X.; Chen, W.; Zu, Z.; Zang, Z.; Deng, M.; Zhu, T.; Sun, K.; Sun, L.; Xue, J. Nanocomposites of AgInZnS and Graphene Nanosheets as Efficient Photocatalysts for Hydrogen Evolution. *Nanoscale* **2015**, *7*, 18498−18503.
(132) Wang, F.; Zheng, M.; Zhu, C.; Zhang, B.; Chen, W.; Ma, L.; Shen, W. Visible Light Photocatalytic H_2-Production Activity of Wide Band Gap ZnS Nanoparticles Based on the Photosensitization of Graphene. *Nanotechnology* **2015**, *26*, 345402.
(133) Zhou, J.; Tian, G.; Chen, Y.; Meng, X.; Shi, Y.; Cao, X.; Pan, K.; Fu, H. In Situ Controlled Growth of $ZnIn_2S_4$ Nanosheets on Reduced Graphene Oxide for Enhanced Photocatalytic Hydrogen Production Performance. *Chem. Commun.* **2013**, *49*, 2237−2239.
(134) Zeng, P.; Zhang, Q.; Peng, T.; Zhang, X. One-Pot Synthesis of Reduced Graphene Oxide−Cadmium Sulfide Nanocomposite and Its

Photocatalytic Hydrogen Production. *Phys. Chem. Chem. Phys.* **2011**, *13*, 21496.
(135) Shen, S.; Ma, A.; Tang, Z.; Han, Z.; Wang, M.; Wang, Z.; Zhi, L.; Yang, J. Facile Synthesis of $Zn_{0.5}Cd_{0.5}S$ Ultrathin Nanorods on Reduced Graphene Oxide for Enhanced Photocatalytic Hydrogen Evolution under Visible Light. *ChemCatChem* **2015**, *7*, 609−615.
(136) Yu, J.; Jin, J.; Cheng, B.; Jaroniec, M. A Noble Metal-Free Reduced Graphene Oxide−CdS Nanorod Composite for the Enhanced Visible-Light Photocatalytic Reduction of CO_2 to Solar Fuel. *J. Mater. Chem. A* **2014**, *2*, 3407−3416.
(137) An, X.; Li, K.; Tang, J. Cu_2O/Reduced Graphene Oxide Composites for the Photocatalytic Conversion of CO_2. *ChemSusChem* **2014**, *7*, 1086−1093.
(138) Iwase, A.; Ng, Y. H.; Ishiguro, Y.; Kudo, A.; Amal, R. Reduced Graphene Oxide as a Solid-State Electron Mediator in Z-Scheme Photocatalytic Water Splitting under Visible Light. *J. Am. Chem. Soc.* **2011**, *133*, 11054−11057.
(139) Du, A.; Ng, Y. H.; Bell, N. J.; Zhu, Z.; Amal, R.; Smith, S. C. Hybrid Graphene/Titania Nanocomposite: Interface Charge Transfer, Hole Doping, and Sensitization for Visible Light Response. *J. Phys. Chem. Lett.* **2011**, *2*, 894−899.
(140) Zhang, Y.; Zhang, N.; Tang, Z.-R.; Xu, Y.-J. Graphene Transforms Wide Band Gap ZnS to a Visible Light Photocatalyst. The New Role of Graphene as a Macromolecular Photosensitizer. *ACS Nano* **2012**, *6*, 9777−9789.
(141) Yang, M.-Q.; Xu, Y.-J. Basic Principles for Observing the Photosensitizer Role of Graphene in the Graphene−Semiconductor Composite Photocatalyst from a Case Study on Graphene−ZnO. *J. Phys. Chem. C* **2013**, *117*, 21724−21734.
(142) Lu, K.-Q.; Zhang, N.; Han, C.; Li, F.; Chen, Z.; Xu, Y.-J. Insight into the Origin of Boosted Photosensitive Efficiency of Graphene from the Cooperative Experiment and Theory Study. *J. Phys. Chem. C* **2016**, *120*, 27091−27103.
(143) Akhavan, O.; Ghaderi, E. Toxicity of Graphene and Graphene Oxide Nanowalls Against Bacteria. *ACS Nano* **2010**, *4*, 5731−5736.
(144) Hu, K.; Szkopek, T.; Cerruti, M. Tuning the aggregation of Graphene Oxide Dispersions to Synthesize Elastic, Low Density Graphene Aerogels. *J. Mater. Chem. A* **2017**, *5*, 23123−23130.
(145) Mao, J.; Iocozzia, J.; Huang, J.; Meng, K.; Lai, Y.; Lin, Z. Graphene Aerogels for Efficient Energy Storage and Conversion. *Energy Environ. Sci.* **2018**, *11*, 772−799.
(146) Yang, H.; Li, Z.; Lu, B.; Gao, J.; Jin, X.; Sun, G.; Zhang, G.; Zhang, P.; Qu, L. Reconstruction of Inherent Graphene Oxide Liquid Crystals for Large-Scale Fabrication of Structure-Intact Graphene Aerogel Bulk toward Practical Applications. *ACS Nano* **2018**, *12*, 11407−11416.
(147) Chen, F.; An, W.; Liu, L.; Liang, Y.; Cui, W. Highly Efficient Removal of Bisphenol A by a Three-Dimensional Graphene Hydrogel-AgBr@RGO Exhibiting Adsorption/Photocatalysis Synergy. *Appl. Catal., B* **2017**, *217*, 65−80.
(148) Chen, M.; Zhang, C.; Li, X.; Zhang, L.; Ma, Y.; Zhang, L.; Xu, X.; Xia, F.; Wang, W.; Gao, J. A One-Step Method for Reduction and Self-Assembling of Graphene Oxide into Reduced Graphene Oxide Aerogels. *J. Mater. Chem. A* **2013**, *1*, 2869−2877.
(149) Yang, S.; Zhang, L.; Yang, Q.; Zhang, Z.; Chen, B.; Lv, P.; Zhu, W.; Wang, G. Graphene Aerogel Prepared by Thermal Evaporation of Graphene Oxide Suspension Containing Sodium Bicarbonate. *J. Mater. Chem. A* **2015**, *3*, 7950−7958.
(150) Weng, B.; Xu, Y.-J. What if the Electrical Conductivity of Graphene is Significantly Deteriorated for the Graphene−Semiconductor Composite-Based Photocatalysis? *ACS Appl. Mater. Interfaces* **2015**, *7*, 27948−27958.
(151) Lu, K.-Q.; Xin, X.; Zhang, N.; Tang, Z.-R.; Xu, Y.-J. Photoredox Catalysis over Graphene Aerogel-Supported Composites. *J. Mater. Chem. A* **2018**, *6*, 4590−4604.
(152) Bai, H.; Li, C.; Wang, X.; Shi, G. On the Gelation of Graphene Oxide. *J. Phys. Chem. C* **2011**, *115*, 5545−5551.
(153) Qiu, B.; Xing, M.; Zhang, J. Recent Advances in Three-Dimensional Graphene Based Materials for Catalysis Applications. *Chem. Soc. Rev.* **2018**, *47*, 2165−2216.
(154) Bai, H.; Li, C.; Wang, X.; Shi, G. On the Gelation of Graphene Oxide. *J. Phys. Chem. C* **2011**, *115*, 5545−5551.
(155) Xu, Y.; Sheng, K.; Li, C.; Shi, G. Self-Assembled Graphene Hydrogel via a One-Step Hydrothermal Process. *ACS Nano* **2010**, *4*, 4324−4330.
(156) Wang, R.; Lu, K.-Q.; Zhang, F.; Tang, Z.-R.; Xu, Y.-J. 3D Carbon Quantum Dots/Graphene Aerogel as a Metal-Free Catalyst for Enhanced Photosensitization Efficiency. *Appl. Catal., B* **2018**, *233*, 11−18.
(157) Chen, W.; Yan, L. In Situ Self-Assembly of Mild Chemical Reduction Graphene for Three-Dimensional Architectures. *Nanoscale* **2011**, *3*, 3132−3137.
(158) Chen, Y.; Xie, X.; Xin, X.; Tang, Z.-R.; Xu, Y.-J. $Ti_3C_2T_x$-Based Three-Dimensional Hydrogel by a Graphene Oxide-Assisted Self-Convergence Process for Enhanced Photoredox Catalysis. *ACS Nano* **2019**, *13*, 295−304.
(159) Kurapati, R.; Russier, J.; Squillaci, M. A.; Treossi, E.; Ménard-Moyon, C.; Del Rio-Castillo, A. E.; Vazquez, E.; Samorì, P.; Palermo, V.; Bianco, A. Dispersibility-Dependent Biodegradation of Graphene Oxide by Myeloperoxidase. *Small* **2015**, *11*, 3985−3994.
(160) Gong, X.; Liu, G.; Li, Y.; Yu, D. Y. W.; Teoh, W. Y. Functionalized-Graphene Composites: Fabrication and Applications in Sustainable Energy and Environment. *Chem. Mater.* **2016**, *28*, 8082−8118.
(161) Tung, V. C.; Huang, J.-H.; Kim, J.; Smith, A. J.; Chu, C.-W.; Huang, J. Towards Solution Processed All-Carbon Solar Cells: A Perspective. *Energy Environ. Sci.* **2012**, *5*, 7810−7818.
(162) Yao, C.; Xie, A.; Shen, Y.; Zhu, W.; Zhu, J. Graphene Oxide Used as a Surfactant to Induce the Flower-Like ZnO Microstructures: Growth Mechanism and Enhanced Photocatalytic Properties. *Cryst. Res. Technol.* **2014**, *49*, 982−989.
(163) Pan, X.; Yang, M.-Q.; Xu, Y.-J. Morphology Control, Defect Engineering and Photoactivity Tuning of ZnO Crystals by Graphene Oxide−a Unique 2D Macromolecular Surfactant. *Phys. Chem. Chem. Phys.* **2014**, *16*, 5589−5599.
(164) Zhang, Y.; Zhang, N.; Tang, Z.-R.; Xu, Y.-J. Graphene Oxide as a Surfactant and Support for In-Situ Synthesis of Au−Pd Nanoalloys with Improved Visible Light Photocatalytic Activity. *J. Phys. Chem. C* **2014**, *118*, 5299−5308.
(165) Yang, X.; Li, C.; Wang, J.; Zhang, J.; Wang, F.; Li, R.; Li, C. Graphene Dispersed Bi_2WO_6 Nanosheets with Promoted Interfacial Charge Separation for Visible Light Photocatalysis. *ChemCatChem* **2019**, *11*, 5487−5494.
(166) Radich, J. G.; Krenselewski, A. L.; Zhu, J.; Kamat, P. V. Is Graphene a Stable Platform for Photocatalysis? Mineralization of Reduced Graphene Oxide With UV-Irradiated TiO_2 Nanoparticles. *Chem. Mater.* **2014**, *26*, 4662−4668.
(167) Xiao, J.-D.; Jiang, H.-L. Metal−Organic Frameworks for Photocatalysis and Photothermal Catalysis. *Acc. Chem. Res.* **2019**, *52*, 356−366.
(168) Cho, Y.-J.; Kim, H.-i.; Lee, S.; Choi, W. Dual-Functional Photocatalysis Using a Ternary Hybrid Of TiO_2 Modified With Graphene Oxide Along With Pt And Fluoride For H_2-Producing Water Treatment. *J. Catal.* **2015**, *330*, 387−395.
(169) Ton, N. N. T.; Dao, A. T. N.; Kato, K.; Ikenaga, T.; Trinh, D. X.; Taniike, T. One-Pot Synthesis of TiO_2/Graphene Nanocomposites for Excellent Visible Light Photocatalysis Based on Chemical Exfoliation Method. *Carbon* **2018**, *133*, 109−117.
(170) Han, C.; Chen, Z.; Zhang, N.; Colmenares, J. C.; Xu, Y.-J. Hierarchically CdS Decorated 1D ZnO Nanorods-2D Graphene Hybrids: Low Temperature Synthesis and Enhanced Photocatalytic Performance. *Adv. Funct. Mater.* **2015**, *25*, 221−229.
(171) Cao, H.; Zhou, X.; Zheng, C.; Liu, Z. Two-Dimensional Porous Micro/Nano Metal Oxides Templated by Graphene Oxide. *ACS Appl. Mater. Interfaces* **2015**, *7*, 11984−11990.

https://doi.org/10.1021/acsmaterialsau.1c00022
ACS Mater. Au 2021, 1, 37−54

(172) Zhao, Y.; Sun, H.; Liu, L.-M.; Zong, R.; Cao, H.; Zhang, Z.; Wang, X.; Luo, J.; Zhu, J. Nanoframes: Space-Confined Creation of Nanoframes in Situ on Reduced Graphene Oxide. *Small* **2015**, *11*, 1481−1481.
(173) Chen, Z.; Liu, S.; Yang, M.-Q.; Xu, Y.-J. Synthesis of Uniform CdS Nanospheres/Graphene Hybrid Nanocomposites and Their Application as Visible Light Photocatalyst for Selective Reduction of Nitro Organics in Water. *ACS Appl. Mater. Interfaces* **2013**, *5*, 4309−4319.
(174) Ullah, K.; Ye, S.; Zhu, L.; Jo, S. B.; Jang, W. K.; Cho, K.-Y.; Oh, W.-C. Noble Metal Doped Graphene Nanocomposites and Its Study of Photocatalytic Hydrogen Evolution. *Solid State Sci.* **2014**, *31*, 91−98.
(175) Latorre-Sánchez, M.; Primo, A.; García, H. P-Doped Graphene Obtained by Pyrolysis of Modified Alginate as a Photocatalyst for Hydrogen Generation from Water−Methanol Mixtures. *Angew. Chem., Int. Ed.* **2013**, *52*, 11813−11816.
(176) Lavorato, C.; Primo, A.; Molinari, R.; Garcia, H. N-Doped Graphene Derived from Biomass as a Visible-Light Photocatalyst for Hydrogen Generation from Water/Methanol Mixtures. *Chem. - Eur. J.* **2014**, *20*, 187−194.
(177) Chen, C.; Cai, W.; Long, M.; Zhou, B.; Wu, Y.; Wu, D.; Feng, Y. Synthesis of Visible-Light Responsive Graphene Oxide/TiO_2 Composites with p/n Heterojunction. *ACS Nano* **2010**, *4*, 6425−6432.
(178) Yang, M.-Q.; Xu, Y.-J. Photocatalytic Conversion of CO_2 over Graphene-Based Composites: Current Status and Future Perspective. *Nanoscale Horiz.* **2016**, *1*, 185−200.
(179) Kong, T.; Jiang, Y.; Xiong, Y. Photocatalytic CO_2 Conversion: What Can We Learn from Conventional CO_x Hydrogenation? *Chem. Soc. Rev.* **2020**, *49*, 6579−6591.
(180) Hsu, H.-C.; Shown, I.; Wei, H.-Y.; Chang, Y.-C.; Du, H.-Y.; Lin, Y.-G.; Tseng, C.-A.; Wang, C.-H.; Chen, L.-C.; Lin, Y.-C.; Chen, K.-H. Graphene Oxide as a Promising Photocatalyst for CO_2 to Methanol Conversion. *Nanoscale* **2013**, *5*, 262−268.
(181) Shown, I.; Hsu, H.-C.; Chang, Y.-C.; Lin, C.-H.; Roy, P. K.; Ganguly, A.; Wang, C.-H.; Chang, J.-K.; Wu, C.-I.; Chen, L.-C.; Chen, K.-H. Highly Efficient Visible Light Photocatalytic Reduction of CO_2 to Hydrocarbon Fuels by Cu-Nanoparticle Decorated Graphene Oxide. *Nano Lett.* **2014**, *14*, 6097−6103.

https://doi.org/10.1021/acsmaterialsau.1c00022
ACS Mater. Au 2021, 1, 37−54